ACS Sustainable Chemistry & Engineering

pubs.acs.org/journal/ascecg

Research Article

Green Design of Renewable Dual-Curing Polymers with Self-Healing and Recyclable Networks for 3D Printing

Rafael T. Alarcon,* Alberto Cellai, Matilde Porcarello, Bernhard Sölle, Elisabeth Rossegger, Carla C. Schmitt, and Marco Sangermano*

Cite This: *ACS Sustainable Chem. Eng.* 2025, 13, 16136−16153

Read Online

ACCESS | Metrics & More | Article Recommendations | Supporting Information

ABSTRACT: This work presents a green design approach for a novel class of dual-curing, self-healing polymers derived from vegetable oils for additive manufacturing. The polymer network is constructed from methacrylated and epoxidized monomers derived through environmentally friendly transformations, allowing for UV-curing radical polymerization followed by thermal curing via acid−epoxy reactions. The resulting materials exhibit self-healing behavior, supporting thermal reprocessing and chemical recycling via transesterification. Designed for circularity, polymers containing the vegetable oil derivatives—methacrylated and epoxidized—reached a biobased content of up to 98% and a biobased carbon content above 77%, far exceeding industry standards. The materials also display alkaline hydrolytic degradation, aligning with end-of-life strategies under a circular economy model. Dual-curing systems achieved an epoxy conversion of over 90% and gel contents above 97%, resulting in stable polymer networks suitable for reprocessing. The formulations were successfully processed using 3D printing platforms, producing well-defined structures despite viscosities exceeding the ideal printability window. The system containing the maleinized/methacrylated grapeseed oil and epoxidized castor oil showed the most favorable behavior, with lower overcuring and the lowest critical energy (37 mJ cm^{-2}). Successful printing confirms the applicability of these systems.

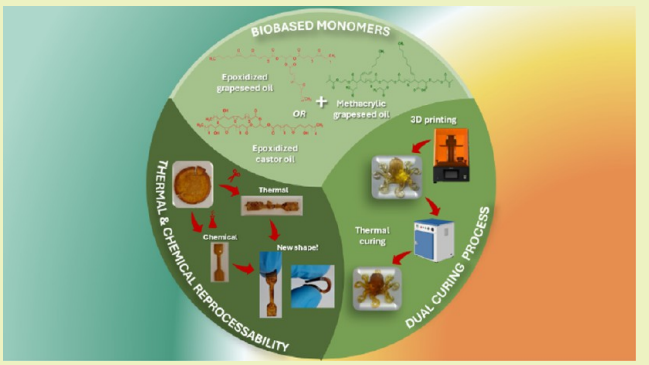

KEYWORDS: *photopolymerization, epoxidized vegetable oil, additive manufacturing, green-design, green chemistry, lipidic biomass*

INTRODUCTION

It is widely recognized that we live in an era dominated by polymers, which play a crucial role in our daily lives, providing essential materials for various applications, including structural, scientific, medical, and technological purposes.[1−10] As a result, polymer production is a major concern today and is expected to reach a staggering 1.2 billion tons by 2060.[11] However, the production of polymers still relies heavily on nonrenewable resources, such as petrochemical derivatives, which account for around 90% of total production. This not only depletes natural resources but also releases harmful gases during the conversion of petrochemical derivatives into monomers and polymers.[12−14] Moreover, only a small percentage of polymeric materials, approximately 10%, are recycled, and the remaining materials are often irregularly discarded in landfills or incinerated, contributing to environmental pollution.[12−14]

Consequently, research in the field of polymers should focus on developing new materials from renewable sources, which aligns with the principles of a circular economy. This concept encompasses four main points: optimizing resource use, reusing and remanufacturing, recycling and recovering materials, and servitization. These points align with the principles of Green Chemistry and the United Nations Sustainable Development Goals (UNSDGs) (e.g., Goal 9 − Industry, Innovation, and Infrastructure; Goal 12 − Responsible Consumption and Production; and Goal 13 − Climate Action), providing a strong foundation for the synthesis of green design in polymers.[12−21]

The polymeric green-design synthesis must be developed, considering clean procedures, the use of renewable chemicals, safe solvents, minimal purification steps, short synthetic times, low energy consumption, higher biobased and carbon content in the final material, material recovery, and polymer degradability at the end of life.[22−31] Therefore, this work presents a green-design synthesis for polymers, taking into account all the aspects mentioned above and adhering to the principles of green chemistry (GC) and the circular economy. First, the green design synthesis begins with the selection of chemical feedstock, which should be renewable rather than

Received: July 16, 2025
Revised: September 9, 2025
Accepted: September 9, 2025
Published: September 15, 2025

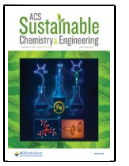

https://doi.org/10.1021/acssuschemeng.5c07154
ACS Sustainable Chem. Eng. 2025, 13, 16136−16153

depleting, if technically and economically feasible (GC principle 7).

In this sense, vegetable oil was chosen as the primary compound because it serves as a versatile and relatively inexpensive chemical building block for monomers and polymers, after a modification process.[32] Therefore, the epoxidized and methacrylated monomers can be used as sustainable 3D resins, adhesives, and functional materials.[28−43] The vegetable oil consists of a glycerol backbone that reacts with three fatty acid chains, creating an ester of glycerol (triacylglycerol or triglyceride).[32,44] The fatty acid chains may contain alkene groups (unsaturated) or not (saturated); however, for the polymer industry, unsaturated vegetable oils are preferred.[32,44] This compound can be extracted from the seeds of various botanical species and is therefore considered a biomass−renewable feedstock (lipidic biomass).[32,44] Consequently, grapeseed oil (GSO) and castor oil (CO) were selected for this purpose since GSO is obtained from the waste seeds of the juice and wine industry, approximately 20% at the end of the process,[36,44,45] and CO is produced in large quantities for technological applications that do not compete with the food industry.[32,46]

The GSO and maleic anhydride were subjected to a pericyclic reaction (Alder-ene) under thermal conditions, resulting in the formation of maleinized oil. This procedure was executed employing microwave irradiation, which operates 12 times more rapidly and utilizes 6 times less energy compared to conventional heating methods.[45,47] Designed for energy efficiency (Principle 6), this approach also achieves a 100% atom economy (Principle 2). Additionally, maleic anhydride is presently synthesized as a renewable chemical from *n*-butane or butyl alcohol and oxygen gas in the presence of vanadium phosphorus oxides (catalyst) or using furfural derivatives.[48−54]

Subsequently, the maleinized oil was reacted with 2-hydroxyethyl methacrylate (HEMA) to obtain a methacrylic derivative (MAGSO); this reaction also demonstrates an atom economy of 100%, as the alcohol from HEMA reacts with the anhydride pendants through nucleophilic acyl substitution.[55−60] HEMA was chosen for this study as it can be regarded as biobased, considering that the ethylene glycol is produced indirectly via the fermentation of xylose from *Escherichia coli*, and the methacrylic acid can be obtained from the catalytic oxidative dehydrogenation of isobutyric acid, a biosynthetic compound.[61,62]

The GSO and CO were similarly subjected to epoxidation through an environmentally friendly procedure that utilizes acetic acid, hydrogen peroxide, and a heterogeneous acid catalyst (Amberlite IR120). This reaction is conducted under moderate conditions (60 °C) without the presence of a solvent.[63] Within just 3 h, the final conversion rate can exceed 95% without parallel reactions.[63] This methodology was developed with a focus on energy efficiency, incorporating less hazardous chemicals (Principle 3) and a catalyst (Principle 4), while also prioritizing safer prevention measures (Principle 12).

Considering the monomers used, the MAGSO is applicable in photopolymerization processes that adhere to the principle of energy efficiency. Moreover, photopolymerization is employed in additive manufacturing, particularly in 3D printing techniques such as stereolithography (SLA) and digital light processing (DLP), which command a market exceeding $11 billion.[64] This methodology presents a significant advantage in the fabrication of sophisticated structures with high resolution, as the polymerization is conducted layer by layer with precisely controlled thickness and exposure duration.[38,64−72]

Nevertheless, the MAGSO, in conjunction with epoxidized vegetable oils, can be utilized in dual-cure materials. To elaborate, the monomeric formulation can initially undergo exposure to light in a free radical polymerization (FRP) process to establish the initial polymeric structure. Subsequently, this polymeric material is subjected to heating to facilitate thermal curing between carboxylic acid (derived from anhydride moieties) and epoxy groups, thereby resulting in a more cross-linked material. The dual-curing process has been extensively researched to develop materials with diverse properties, including fluorescence, shape memory, conductivity, and healing capabilities.[73−84]

Furthermore, the polymer has been engineered to exhibit self-healing properties following the dual-curing process; in other words, these materials are recognized as Covalent Adaptable Networks (CANs).[32,42,85,86] CANs are characterized by covalent cross-links similar to those found in thermosets; however, they demonstrate reversible dynamics when exposed to stimuli such as heat, pressure, light, or changes in pH.[7,29,35,87−90] In the absence of these stimuli, CANs maintain thermoset-like properties.[32,42,85,86] Additionally, CANs have the potential for recyclability due to their dynamic cross-linking composition. Therefore, after the reaction between carboxylic acid and epoxy groups, new alcohol groups are formed. These can engage in a transesterification reaction to heal the polymeric matrix in the presence of a catalyst. This reaction is considered an associative mechanism since the cross-linking remains constant.[32,42,85,86] CANs materials align with the principles of recycling, recovery, and servitization emphasized by the circular economy.

Lastly, the final polymer was designed to hydrolyze in alkaline environments, thereby reducing its accumulation in the environment.[29−31,91−93] This process readily occurs with the ester groups from the glycerol backbone and those newly formed after the polymerization reactions.[29,31] This point aligns with the design of degradation (principle 10) and the circular economy.

This work emphasizes a comprehensive green-design strategy for synthesizing renewable networks, incorporating clean synthetic methods, energy-efficient techniques, dual-curing strategies, and dynamic covalent adaptable networks. The developed polymeric materials are suitable for 3D printing applications and exhibit reprocessability as well as chemical degradation in alkaline conditions. These characteristics position these systems as promising candidates for sustainable polymers that align with the principles of green chemistry, the circular economy, and the United Nations Sustainable Development Goals.

EXPERIMENTAL SECTION

Materials. Vegetable oils from grapeseed-GSO (batch code: pe036/22) and castor-CO (batch code: 12−60319) were acquired from Mundo dos Óleos (Brazil). Glacial acetic acid (≥99), Amberlite IR-120, hydrogen peroxide (30%, H_2O_2), ethyl acetate, toluene, diethyl ether, maleic anhydride (99%), 2-hydroxyethyl methacrylate − HEMA (≥99), hydroquinone (99%), deuterated chloroform ($CDCl_3$, 99.8% D) containing tetramethylsilane (TMS), and the photoinitiator phenylbis(2,4,6-trimethylbenzoyl)phosphine oxide − BAPO

https://doi.org/10.1021/acssuschemeng.5c07154
ACS Sustainable Chem. Eng. 2025, 13, 16136−16153

Table 1. Mass of Maleinized/Methacrylated Grapeseed Oil-MAGSO, Epoxidized Grapeseed Oil−EGSO or Epoxidized Castor Oil-ECO, and Photoinitiator (BAPO) for Each Formulation[a]

Formulation	MAGSO (g)	EGSO (g)	ECO (g)	BAPO (g)
MAGSO-B	4.0000	-	-	0.0800
MAGSO-C	4.0000	-	0.8296	0.0966
MAGSO-G	4.0000	0.6765	-	0.0935

[a]Weighed in an analytical balance with a precision of ±0.1 mg.

(97%) were purchased from Sigma-Aldrich and used without further purification. The eugenol phosphate (EUGP) was kindly given by Polymer Competence Center Leoben GmbH − PCCL.

Characterization of Each Vegetable Oil and Monomers By ^{1}H NMR. The vegetable oils CO and GSO were first characterized by^1 H NMR to determine the iodine value (IV), the average number of alkenes ($DB_{average}$), and the number of alkenes per 100 g of sample; these parameters are important for further reactions. Therefore, the ^{1}H NMR spectra of the vegetable oil were obtained using a 400 MHz Agilent Premium Shield spectrometer, with $CDCl_3$ as the solvent.

The IV was determined using eq 1, by the integration of the multiplet at 5.36 ppm for GSO or multiplets at 5.35 and 5.55 ppm for CO. These signals are related to vinyl hydrogens, after the normalization process by the signal of hydrogens related to α-carbonyl (total of six hydrogens) at 2.31 ppm, then given the K value.[94]

The number of alkenes per 100 g of oil (mol) was determined by dividing the IV per the molar mass of I_2 (253.808 g mol^{-1}). The $DB_{average}$ was determined by eq 2, the Nf is associated with four hydrogens attached to the glycerol backbone (4.14 and 4.29 ppm) divided by the number of related hydrogens (4 hydrogens).[94]

$$IV = \frac{(12691 \times K)}{(821.3 + 6.006 \times K)} \quad (1)$$

$$DB_{average} = \frac{K}{2Nf} \quad (2)$$

The epoxidation conversion was verified by monitoring signals related to vinyl hydrogens in each vegetable oil, as well as a new signal between 2.87 and 3.21 ppm.[94] For the maleinization process, the integral related to vinyl hydrogen was also monitored, together with new signals at 2.17, 3.22, 5.60, 5.91, and 6.46 ppm, which were related to hydrogens attached to anhydride pendants.[45,95]

For the methacrylate reaction, new signals at 5.58 and 6.12 ppm were monitored since they are related to hydrogens attached to the methacrylic group. Then, the average quantity of methacrylate groups (MAG) per triacylglycerol molecule was calculated by using eq 3, in which MAH is the total area for the signals between 5.58 and 6.12 ppm, and (∝H) is the area of α-carbonyl hydrogens at 2.31 ppm.[96,97]

$$MAG = \frac{MAH}{\left(\frac{aH}{6}\right)} \quad (3)$$

Epoxidation Reaction. The GSO and CO were epoxidized following the procedure described in the literature.[63] The mol ratio between alkenes in each vegetable oil, hydrogen peroxide, and glacial acetic acid was equal to 1:6:1. Amberlite IR-120 (catalyst) was used in a ratio of 10 wt % to the mass of vegetable oil. All reactants were added to a round-bottomed flask equipped with a reflux system; thereafter, the reaction was executed at 60 °C for 3 h under constant stirring. Subsequently, the crude product was filtered to remove the heterogeneous catalyst and then added to a separatory funnel along with 100 mL of ethyl acetate. This solvent is green and recommended by the CHEM21 selection guide of classical and less classical solvents.[98]

The organic phase was washed with a hydrogen carbonate solution (0.1 mol L^{-1}) to remove residual acid, and then with brine (50 mL) to facilitate separation. The organic phase was dried with anhydrous magnesium sulfate and filtered again to remove the drying agent. Lastly, the organic phase was added to a round-bottomed flask, and the ethyl acetate was removed using a rotary evaporator, resulting in the final product. ECO is a colorless oil and a white paste at room temperature, while EGSO is a white, greasy compound at room temperature.

Maleinization Reaction. The GSO was maleinised following a procedure reported in the literature.[47] The maleinisation process was executed in a microwave oven with a Teflon reactor, which has a manometer and is connected to a thermocouple. Therefore, 50 g of GSO was added to the reactor together with 25 g of maleic anhydride. The system was controlled by software (Incon V 1.5) in temperature mode, and therefore was heated up to 235 °C at a heating rate of 10 °C min^{-1}, and then maintained for 15 min. Subsequently, the system was cooled to room temperature, and 50 mL of cold toluene (less hazardous than hexane, as reported in CHEM 21)[98] was added to the crude product, resulting in the precipitation of maleic anhydride. The system was then filtered, and the toluene was removed using a rotary evaporator, resulting in an orange oil product (MGSO). After the purification step, the quantity of maleic anhydride incorporated into the oil structure was determined by titration (3×), as described in the literature.[45,47] The anhydride content was equal to 0.0835 ± 0.0003 mol of anhydride per 100 g of sample.

Methacrylation Reaction. The methacrylation reaction was performed according to a procedure reported in the literature with some adaptations.[56] The MGSO (100 g), hydroquinone (inhibitor, 5%), and HEMA (0.09 mol) were added to a round-bottomed flask attached to a reflux system. The reaction was executed for 12 h at 100 °C under constant stirring. Thereafter, the system was cooled down, and the crude product was transferred to a separatory funnel, and 100 mL of diethyl ether was added. This solvent was selected due to its low boiling point; another option would be dichloromethane (DCM). However, we preferred to work with a solvent that does not contain halogens.[98] The organic layer was washed 5 times with distilled water (50 mL) and with brine (50 mL) to assist layer separation. Thereafter, the organic phase was dried with anhydrous magnesium sulfate and filtered again to remove the drying agent. Lastly, the organic phase was added to a round-bottomed flask, and the diethyl ether was removed using a rotary evaporator, resulting in the final product: a dark-orange, viscous oil − maleinized/methacrylated grapeseed oil (MAGSO).

Resin Formulations, Photopolymerization Conversion, and Thermal Curing. Three different formulations were prepared using the MAGSO. The first formulation contains MAGSO as monomers and BAPO as photoinitiator (2 parts per hundred of resin-phr); this sample is the blank

https://doi.org/10.1021/acssuschemeng.5c07154
ACS Sustainable Chem. Eng. 2025, 13, 16136−16153

(**MAGSO-B**). The other two formulations contain MAGSO, ECO (**MAGSO-C**), or EGSO (**MAGSO-G**) as epoxy monomers in an equimolar ratio of functional groups, along with BAPO photoinitiator (2 phr). These components were added to different opaque flasks, then manually stirred and settled in an ultrasonic bath at 60 °C for 20 min, resulting in a homogeneous mixture. All the investigated formulation compositions are reported in Table 1.

The photopolymerization process was performed using a LightCuring LC8 (Hamamatsu Photonics) with an intensity of 15% (80 mW cm^{-2}, 365 nm), and each formulation was spread onto a Si substrate with a layer thickness of 12 μm. The spectrum was obtained at different times (0, 10, 20, 30, 60, 90, and 120 s) using a Nicolet iS10 spectrometer from Thermo Scientific, within a spectral range of 4000 to 500 cm^{-1} (resolution of 4 cm^{-1}). Conversions were determined using eq 4, monitoring the area of the band at 1625 cm^{-1}, which is related to the C = C bond of the methacrylic group (A_{group}). To normalize the spectrum, the band at 1738 cm^{-1} associated with C = O stretching from the backbone glycerol ester was also monitored (A_{ref}).[28,46] The conversion was performed in triplicate.

$$C(\%) = \frac{\left(A_{group}/A_{ref}\right)_{t=0} - \left(A_{group}/A_{ref}\right)_{t=x}}{\left(A_{group}/A_{ref}\right)_{t=0}} \times 100 \quad (4)$$

The rate of polymerization (Rp, mol s^{-1}) was calculated using eq 5 for each formulation system at different times (0, 10, 20, 30, 60, 90, and 120 s), then providing the rate curve. Where $[x_0]$ is the molar fraction of methacrylic monomer, Δ_A is the difference between two areas related to the C═C of the methacrylic group at 1625 cm^{-1}, A_0 is the initial area at a time equal to zero, and Δ_t is the time difference between two analyses.[28,46]

$$R_p = [x_0] \times \left[\frac{\Delta_A}{A_0 \times \Delta_t}\right] \quad (5)$$

For thermal investigation, the formulations MAGSO-C and MAGSO-G were photopolymerized in a silicon mold (ϕ10 mm × 1 mm thickness) for 120 s using a LightCuring LC8 (Hamamatsu Photonics) with an intensity of 15% (80 mW cm^{-2}). Thereafter, these samples were subjected to thermal curing at 130 °C for different times (30, 60, 120, 180, 240, and 300 min), resulting in the thermal-cured polymers MAGSO-CT and MAGSO-GT. Conversions were performed in triplicate and determined using eq 4, monitoring the area of the two close bands at 822 cm^{-1} and 845 cm^{-1}, which are related to the epoxy group (A_{group}). To normalize the spectrum, the band at 2850 cm^{-1}, associated with C−H stretching (Aref), is used. The equipment was the same as previously mentioned; however, the spectra were obtained by attenuated total reflectance mode (ATR) using a diamond window (4000 to 500 cm^{-1} and resolution of 4 cm^{-1}).

Differential Scanning Calorimetry (DSC), Photo-DSC, and Thermogravimetry (TG). The differential scanning calorimetry (DSC) analyses for each polymer were performed using a DSC-1 modulus (Mettler-Toledo) with 8.0 mg of samples in 40 μL aluminum crucibles and a perforated lid. The curve was recorded in the range of −50 to 150 °C under a nitrogen flow rate of 40 mL min^{-1} for the determination of the glass transition temperature (T_g).

The photo-DSC curves were acquired using the same equipment and parameters, except for the temperature, which was maintained at 25 °C (isothermal mode). Each photocurable formulation resins were photopolymerized using LightCuring LC8 (Hamamatsu Photonics) with an intensity of 15% (80 mW cm^{-2}, 365 nm). To obtain the pure exothermic photopolymerization curve, two isothermal cycles were recorded. Then, the second curve was subtracted from the first one, and both were irradiated with UV light. Therefore, the enthalpy (ΔH) for each system was obtained.

Thereafter, the conversion for each photocurable formulation was calculated by eq 6 The ΔH_{total} is the enthalpy for a conversion of 100% cross-linking, and dH/dt is the heat flow under a specific isothermal condition, in this case, at 25 °C.[97,99]

$$C = \frac{1}{\Delta H_{total}} \times \int_t^0 \left(\frac{dH}{dt}\right) T \quad (6)$$

The rate of polymerization (Rp, s^{-1}) for the maximum value of the peak was also calculated for each photocurable formulation from eq 7[97,99]

$$R_p = \frac{1}{\Delta H_{total}} \times \left(\frac{dH}{dt}\right)_T \quad (7)$$

Polymers were subjected to simultaneous thermogravimetry-differential scanning calorimetry (TGA/DSC) using a TGA/DSC 3^+ Star^e System simultaneous module (Mettler-Toledo). Samples (9.0 mg) were placed into an α-alumina open crucible (200 μL). The temperature range was from 30 to 800 °C in a heating rate of 10 °C min^{-1} under a dynamic dry air atmosphere (50.0 mL min^{-1}).

Stress-Relaxation Analysis. Stress-relaxation behaviors of the UV-cured samples after thermal treatment (3 h at 130 °C − MAGSO-CT and MAGSO-GT) and containing 15 phr of transesterification catalyst (Eugenol phosphate -EUGP) were determined using a MCR 302e rheometer from Anton Paar. The sample dimension had an average diameter of ϕ25 mm and a thickness of 1 mm. The sample was first preloaded with a normal force of 1 N applied for 15 min at the set temperature. A constant 3% strain was applied, and the variation of the relaxation modulus was recorded over time. The chosen temperatures corresponded to 150 °C, 160 °C, 170 °C, and 180 °C.

The relaxation data were analyzed with the Kohlrausch−Williams−Watts (KWW, eq 8) function, including an elastic offset to account for the incomplete decay within the time window.[100−102] Where G_∞ is the long-time modulus (offset), A is the amplitude, τ is the characteristic relaxation time (s), and $0< \beta \leq 1$ is the stretch value parameter shape, which can be associated with network homogeneity and reaction processes. For reference, the Debye limit is recovered when $\beta = 1$, giving eq 9[101−104] Defining the normalized relaxation $\phi(t) = (G(t)—G_\infty)/A$, the time τ corresponds to the instant at which $\phi(t) = 1/e$. In practice, τ is obtained from the global fit of eq 9, not by reading the raw curve at 1/e.

$$G(t) = G_\infty + Ae^{\left[\left(-\frac{t}{\tau}\right)^\beta\right]} \quad (8)$$

$$G(t) = G_\infty + Ae^{\left(-\frac{t}{\tau}\right)} \quad (9)$$

https://doi.org/10.1021/acssuschemeng.5c07154
ACS Sustainable Chem. Eng. 2025, 13, 16136−16153

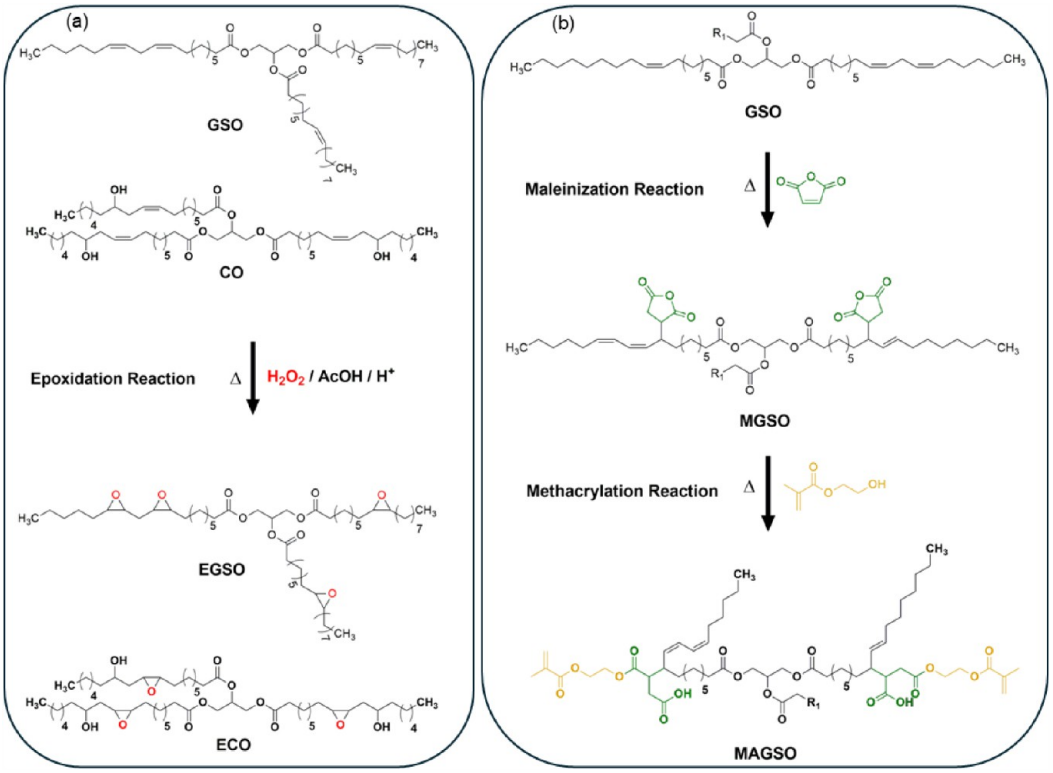

Figure 1. Vegetable oil functionalization by (a) epoxidation reaction, and (b) maleinization followed by methacrylation reaction.

The τ was analyzed by Arrhenius, and the activation energy was determined by extrapolating the Arrhenius plot, as per eq 10[100]

$$\ln(\tau) = \ln(\tau_0) + E_a\frac{1000}{RT} \tag{10}$$

Where E_a is the activation energy [J/mol], R is the universal gas constant [J/mol·K], T is the temperature [K], and τ_0 is a pre-exponential factor. By plotting $\ln(\tau)$ vs $1000/T$, it is possible to calculate E_a using eq 11, considering the slope of the curve (a).[100]

$$E_a = a \times 1000 \times R \tag{11}$$

Tensiometric Analysis, Gel Content, Bio-Based Carbon Content, and Bio-Based Content. Contact angles for all polymeric materials were measured using a Kruss DSA10 tensiometer equipped with a digital camera. A drop of water was deposited on the surface of each sample, and 10 optical scans were performed to verify the contact angle formed between the drop and the surface.

For the gel content measurement, about 1.0 g (m_i) of each sample was added to different metallic nets and submerged in chloroform for 24 h. The chloroform was selected since these monomers can be easily solubilized, as it is the same solvent used for ^{1}H NMR analysis. Thereafter, all nets were dried at room temperature for 24 h, and the final mass (m_f) was recorded in an analytical balance. The gel content was calculated using eq 12

$$GC(\%) = \left[\frac{m_f}{m_i}\right] \times 100 \tag{12}$$

Biobased carbon content (BCC) was calculated for each polymer using eq 13[28,29] In this equation, renewable sources are related to carbon from MAGSO, ECO or EGSO, and the catalyst-EUGP $(C_{renewable})$. The nonrenewable source $(C_{nonrenewable})$ is related to those from the BAPO (photoinitiator).

$$BCC\ (\%) = \left[\frac{C_{renewable}}{C_{renewable} + C_{non-renewable}}\right] \times 100 \tag{13}$$

The biobased content (BC) was calculated by eq 14,[28,29] in which m_{MAGSO}, $m_{ECO/EGSO}$, m_{BAPO}, and m_{EUGP} are the masses in grams of maleinized/methacrylic grapeseed oil (MAGSO), epoxidized castor oil (ECO) or epoxidized grapeseed oil (EGSO), photoinitiator (BAPO), and catalyst (eugenol phosphate-EUGP), respectively. The BAPO is not considered renewable.

$$BC(\%) = \left[\frac{m_{MAGSO} + m_{ECO/EGSO} + m_{EUGP}}{m_{MAGSO} + m_{ECO/EGSO} + m_{photo} + m_{EUGP}}\right] \times 100 \tag{14}$$

Viscosity, Working Curves, Printing, and Overcuring Analysis. The viscosity measurements of photocurable formulations were performed in an Anton-Paar Modular Compact Rheometer (model MC 302e) using a plate−plate configuration (metal-based disks with a diameter of 25 mm) with a gap of 0.3 mm. All measurements were performed at room temperature using a shear rate from 0.1 to 1000 s^{-1}.

The working curves for 3D printing were performed for all three photocurable formulations. The curing depth (C_d) and critical energy exposure (E_c) were determined in this investigation conducted in a Phrozen Sonic Mighty 4K 3D printer using the maximum light intensity (E_{max} = 1.9 mW cm^{-2}, 405 nm) at room temperature and at different times (50, 60, 70, 80, 90, 100, 110, and 120 s). Sample thickness was

https://doi.org/10.1021/acssuschemeng.5c07154
ACS Sustainable Chem. Eng. 2025, 13, 16136−16153

measured using a micrometer, resulting in the C_d for each time. The E_c was calculated using eq 15, which is the critical energy for the formulation to reach the gelation state. The term D_p is the depth of resin when the light intensity is reduced to $1/e$ (≈37%) of its incident value (i.e., it can be obtained by the slope inclination of the analytical curve).[28,105−108]

$$C_d = D_p \ln\left(\frac{E_{max}}{E_c}\right) \quad (15)$$

Photocurable formulations were tested for printability with different 3D structures using the same printer mentioned above. The exposure time was 300 s for the five bottom layers and 80 s for the other 50 μm layers. After printing, these structures were removed from the support and submerged in isopropyl alcohol for 5 min in an ultrasonic bath to remove the nonpolymerized residual monomers. Thereafter, the cleaned samples were dried and postcured for 30 min in Phrozen curing station equipment (wavelength = 405 nm).

A test structure containing cavities and walls with defined dimensions was used to evaluate the resolution and overcuring that can directly affect the resolution of 3D-printed objects. The overcuring was determined using eqs 16 or 17.[109,110] Therefore, the calculation considered the cavity radii and wall widths using both theoretical values from the CAD model and empirical measurements from the 3D-printed object. 3D-printed objects were measured using a digital calliper.

$$\%Overcure_{cavity} = \frac{Theoretical - Experimental}{Theoretical} \times 100 \quad (16)$$

$$\%Overcure_{wall} = \frac{Experimental - Theoretical}{Theoretical} \times 100 \quad (17)$$

Thermal Reprocessing, Chemical Recyclability, and Hydrolysis Test. For thermal reprocessing, the MAGSO-C containing EUGP was sliced into small pieces and added onto a silicon mold with a dogbone shape. Thereafter, the mold was placed inside an oven at 150 °C for 3 h, with a metal plate positioned above the mold in contact with the polymer, and a 10 kg metal piece was placed on top to ensure the self-healing process.

The chemical recyclability was performed by adding pieces of MAGSO-G (100 mg) to a vessel containing 10 mL of ethanol and a magnetic stirring bar. Thereafter, the vessel was closed and heated at 50 °C for 6 h. The ethanol was then evaporated under stirring to remove it from the system, resulting in a concentrated mixture of monomeric and oligomeric solutions. This material was poured into the silicon mold with a dogbone shape and thermally treated in the same manner described above.

A hydrolysis test was performed using a NaOH solution (1 mol L^{-1}). All UV-cured polymers, both with and without thermal treatment, were subjected to hydrolysis by immersing them in such a solution for 48 h. Pictures were taken along this process to monitor the hydrolysis.

RESULTS AND DISCUSSION

Vegetable Oil Functionalization. Initially, the raw vegetable oils from grapeseed and castor were characterized by ^{1}H NMR in order to determine the $DB_{average}$, and the mol of alkenes per 100 g of sample, which is determined by the iodine value (IV). The grapeseed oil (Figure S1) has an iodine value of 125.3 g I2 per 100 g sample, corresponding to 0.4937 mol of alkene per 100 g and a DB average of 4.3 per molecule. The castor oil (Figure S2) presents an alkene content of 0.4137 mol per 100 g (IV = 105.0 g I_2 per 100 g sample), and a $DB_{average}$= 3.6 per molecule. The castor oil is mostly composed of ricinoleic oil that presents one alkene per chain; however, by ^{1}H NMR, a triplet signal at 0.98 ppm is exhibited that is associated with methyl hydrogens of the ∝-linolenic chain, and a triplet at 2.77 ppm related to bis-allylic hydrogens.[46]

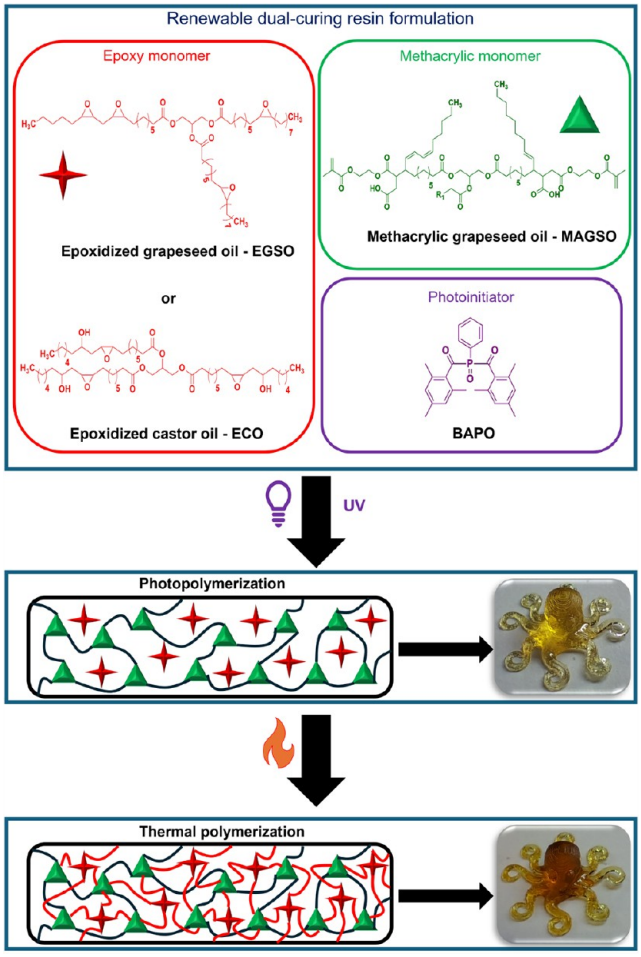

Figure 2. Renewable dual-curing resin formulation from vegetable oil derivatives and the dual-curing process.

Both vegetable oils underwent an epoxidation reaction; hence, the signal at 5.36 ppm for the GSO and the signals at 5.35 and 5.55 ppm for CO, related to vinyl hydrogens, vanished. In contrast, new signals between 2.87 and 3.21 ppm appeared (hydrogens attached to epoxy rings).[45] Therefore, based on these ^{1}H NMR results, the conversion for both systems was ≥ 99%. The ^{1}H NMR spectra for epoxidized grapeseed oil-EGSO and epoxidized castor oil-ECO are displayed in Figures S3 and S4, respectively. These findings are also corroborated by FTIR spectra (Figure S5), which present a band at 1650 cm^{-1} related to C = C stretching and a band at 3010 cm^{-1} related to C−H stretching of alkenes; however, after epoxidation, both bands disappeared, and two new close bands related to the symmetric and asymmetric epoxy ring deformation appeared at 821 cm^{-1} and 844 cm^{-1}.[45,94] The epoxidation reaction for ECO and EGSO is displayed in Figure 1a.

The GSO was also reacted with maleic anhydride to produce the maleinised oil. This process occurs preferentially through a

https://doi.org/10.1021/acssuschemeng.5c07154
ACS Sustainable Chem. Eng. 2025, 13, 16136−16153

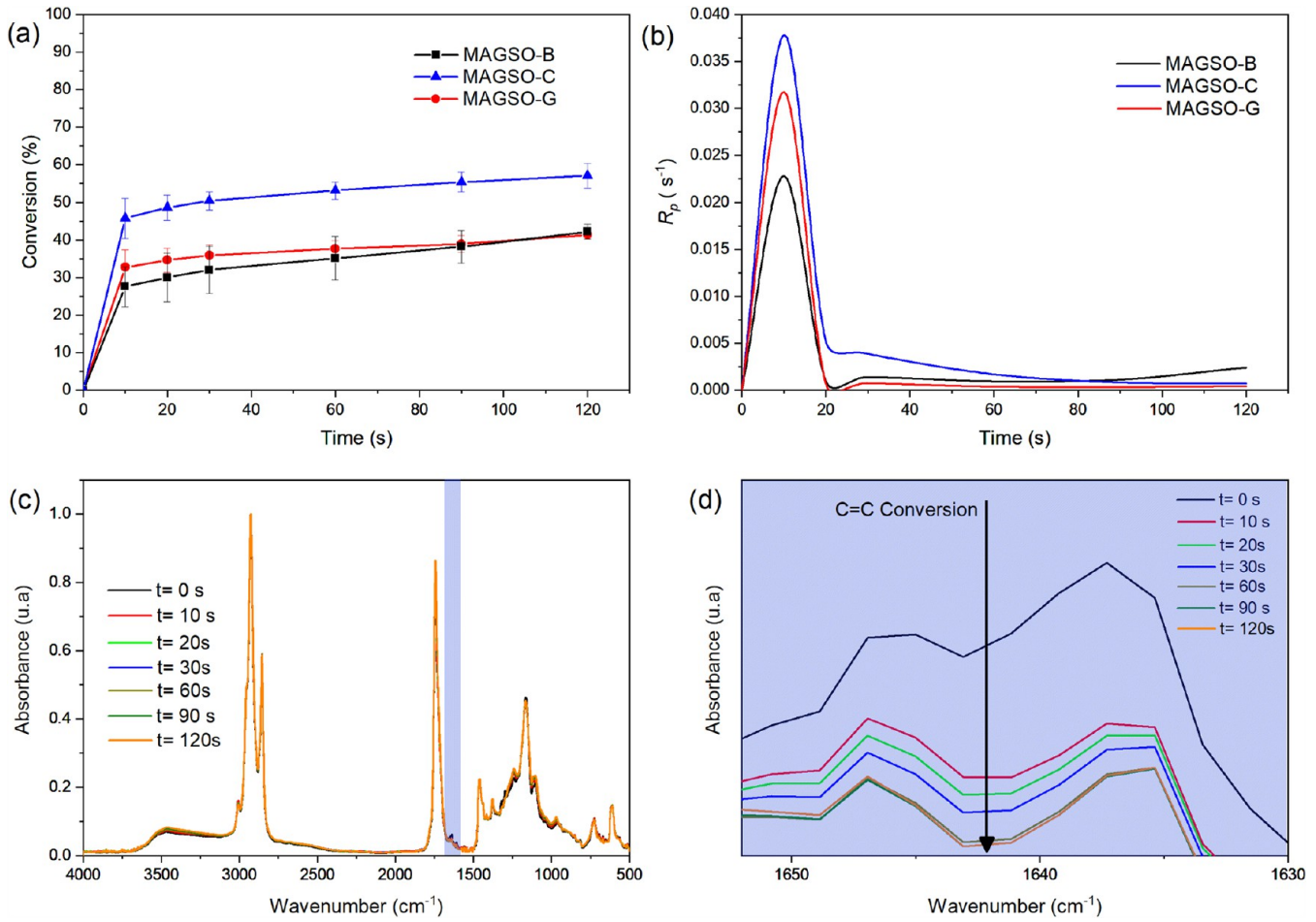

Figure 3. (a) Conversion of methacrylic double bonds (C═C) for each photocurable resin at different times, (b) rate of polymerization for each photocurable resin, (c) FTIR spectra for MAGSO-C, and (d) amplified FTIR spectra in the methacrylic double bonds band at different times.

pericyclic reaction (Alder-Ene), adding a pendant anhydride to the fatty chain; however, the addition can also occur via a radical process or by radical deprotonation.[45,47,95] These three reactions occurred, as confirmed by ^{1}H NMR (Figure S6). The signals at 2.17, 3.22, and 5.91 ppm confirm the type ene reaction.[45,95] The appearance of new signals at 2.43 and 2.65 ppm, together with the diminishing of hydrogens related to alkenes at 5.36 ppm, indicates the radical reaction.[45,95] Furthermore, the signals at 5.60, 5.91, and 6.46 ppm indicate the radical deprotonation and Diels−Alder adduct that is formed between the isomerized linoleic or ∝-linolenic chains (diene) and maleic anhydride (dienophile).[45,95] The FTIR spectrum (Figure S7) for maleinised oil presents new bands at 1707 cm^{-1} and 1777 cm^{-1}, which are associated with the symmetric and asymmetric C═O stretching in anhydride pendant; moreover, the small band at 1857 cm^{-1} is related to an overtone of the band at 919 cm^{-1} (ring deformation).[45]

Thereafter, the maleinized oil was reacted with HEMA to produce the methacrylated oil (MAGSO). Signals at 5.58 and 6.12 ppm are related to vinyl hydrogens of the methacrylic pendant, and the signals 3.45 and 3.86 ppm are associated with hydrogens of the ethylene glycol backbone (Figure S8).[111] By using eq 3, it is possible to determine the average quantity of methacrylic pendants, which was equal to 2 units per molecule of triacylglycerol. The FTIR spectrum for MAGSO (Figure S9) presents the vanishing of bands related to the C═O stretching of anhydride. Still, a new band at 1635 cm^{-1} is presented, which is related to the C═C stretching of the methacrylic pendant.[111] The maleinization and methacrylation reactions are exhibited in Figure 1.

Cross-Linking Reaction and Characterization. The polymerization using MAGSO occurs through UV light curing via free radical polymerization (FRP). Consequently, the photoinitiator is excited by the light, forming radicals that trigger the reaction by adding the double bonds of the methacrylic pendants.[112,113] This process promotes the cross-linking reaction.

However, when the epoxidized monomer is present in the system, a second cure can occur through a subsequent thermal process. Therefore, formulations containing epoxidized grapeseed oil (EGSO) or castor oil (ECO) can undergo a dual-cure process. After the UV-curing process, the thermal post-treatment involves the carboxylic acid attacking the epoxy rings through an S_N2 reaction, resulting in the formation of ester and alcohol groups.[30,36,114] Figure 2 displays the photocurable formulations and the dual-cure process.

These formulations were designed to have a higher biobased content (BC) and biobased carbon content (BCC). All formulations presented BC values equal to 98% and BCC values higher than 63%. This outcome can be attributed to the renewable nature of the monomer already discussed in this study. Therefore, the MAGSO-B presented a BC value of 98.0% and a BCC value of 63.1%. In contrast, the MAGSO-C presented a higher value related to the BC (98.3%) due to the

https://doi.org/10.1021/acssuschemeng.5c07154
ACS Sustainable Chem. Eng. 2025, 13, 16136−16153

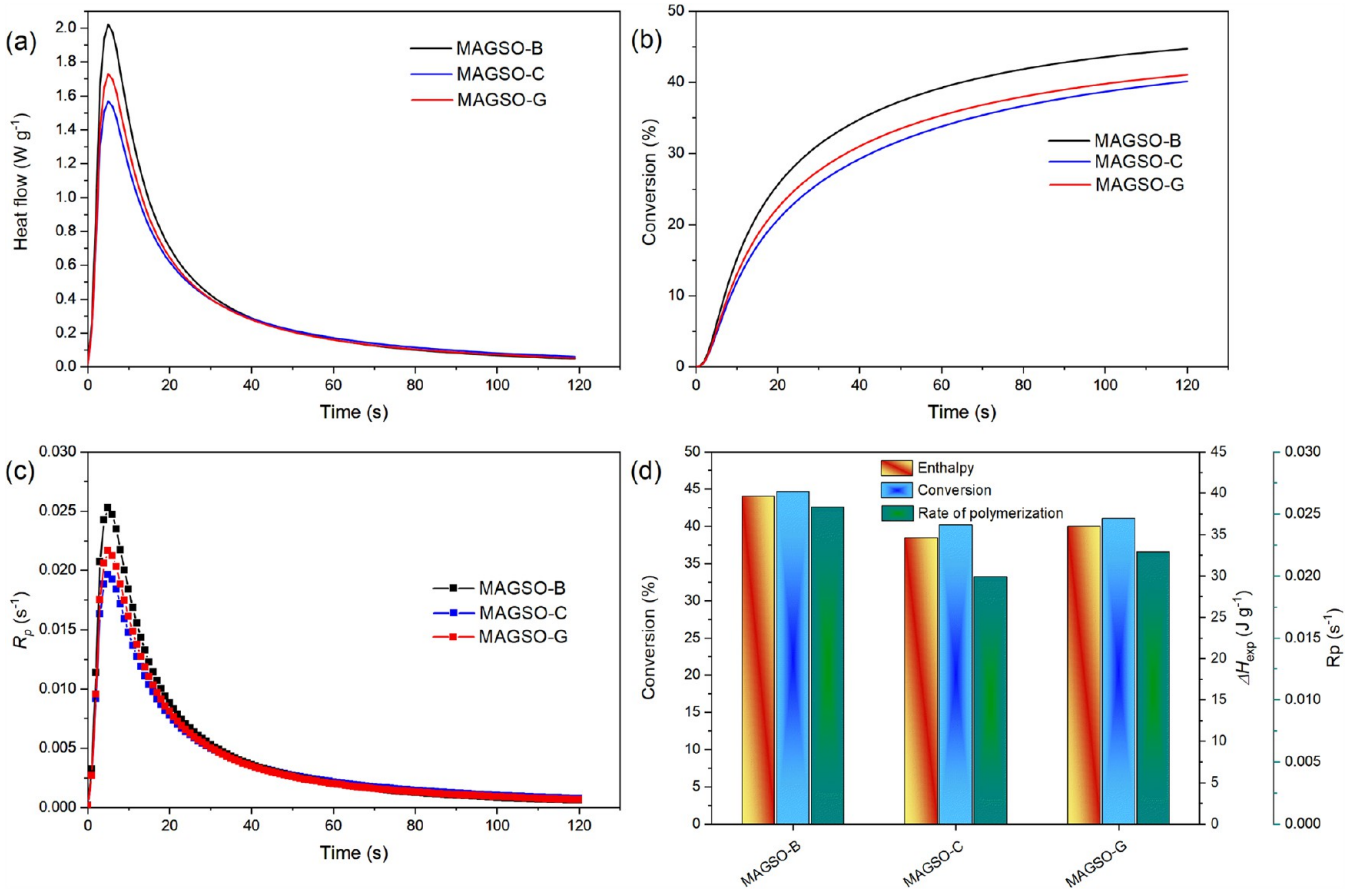

Figure 4. (a) DSC curves of polymerization for each photocurable formulation, (b) conversion curves, (c) rate of polymerization curves, and (d) compilation of all results.

presence of the renewable catalyst, Eugenol phosphate (EUGP), which will be exploited in the dynamic covalent network process. Moreover, the BCC value was equal to 77.6%, which is higher than that of MAGSO-B (63.1%). The same findings are seen for the MAGSO-G with a BC value of 98.3% and a BCC value of 77.6%.

Polymers should have a minimum value of 25% for BC and BCC to be considered a renewable, green material.[115−117] Most commercial biobased epoxy formulations fail to meet this minimum requirement.[115−117] Consequently, the systems presented here, in addition to their suitability as a photopolymerizable resin, exhibit an ideal green aspect.

First, the conversion was studied using FTIR (Figure 3a). The MAGSO-B presented a maximum acrylic double bond conversion of 42 ± 2% after 120 s, which is similar to that found for MAGSO-G (41 ± 1%). The highest conversion is observed for the MAGSO-C (57 ± 3%). The maximum rate of polymerization (R_p, Figure 3b) at 10 s is also observed for the MAGSO-C (0.038 s^{-1}), followed by the MAGSO-G (0.032 s^{-1}), and last for the MAGSO-B (0.022 s^{-1}). These results indicate that the addition of epoxidized monomers has a positive effect on photopolymerization, which can be attributed to an increase in the interaction between MAGSO and epoxy monomers. This effect was also observed in the working curves and critical energy, which will be further discussed in the topic about 3D printing.

All spectra for MAGSO-C at different irradiation times are displayed in Figure 3c. The band related to the double bond from methacrylate is observed between 1630 and 1650 cm^{-1}. This band is related to the C═C stretching and appears as two overlapped bands because the methacrylic, which is ∝,β-unsaturated ester, causes a resonance effect with the carboxylic.[28,111] As expected, with the progression of the photopolymerization, the bands are reduced, and it is more evident when the region is magnified (Figure 3d).

All photocurable formulations were analyzed by photo-DSC (Figure 4a) to determine the polymerization peak time under UV light, the experimental enthalpy of the reaction (ΔH), and from this, the conversion curve (Figure 4b) and the rate of polymerization (Figure 4c). The compilation of these results is shown in Figure 4d.

These formulations exhibited the same maximum polymerization after 5 s of UV irradiation, indicating that the reaction proceeds at a rapid rate. The highest ΔH is observed for the MAGSO-B (39.6 J g^{-1}), followed by the MAGSO-G (37.0 J g^{-1}) and MAGSO-C (35.6 J g^{-1}). From the DSC curve, it was possible to calculate the conversion curve using eq 6 and considering the theoretical enthalpy of reaction as 97.2 kJ per methacrylated group. As expected from the enthalpy, the MAGSO-B showed the highest conversion (41%), followed by MAGSO-G (37%) and MAGSO-C (36%). As can be seen, all conversions are close to each other but are lower than those observed by the FTIR. This can be explained by the difference in layer thickness in each analysis, as the FTIR utilizes a layer thickness of 12 μm. In contrast, the DSC uses a higher layer thickness, even with low mass loading. However, the findings of DSC and FTIR are still in good agreement. Table 2 reports all findings obtained by FTIR and DSC.

https://doi.org/10.1021/acssuschemeng.5c07154
ACS Sustainable Chem. Eng. 2025, 13, 16136−16153

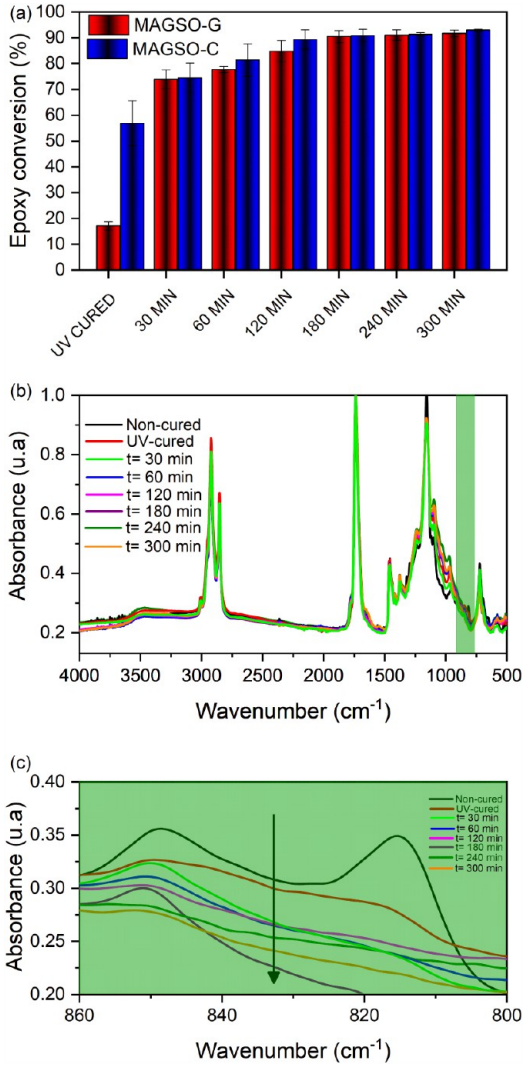

Figure 5. (a) thermal curing over time for MAGSO-C and MAGSO-G, (b) FTIR spectra for MAGSO-C, and (c) amplified FTIR spectra in the epoxy bands at different times.

After investigating the conversion through UV curing, the thermal conversion of the MAGSO-C and MAGSO-B samples was examined (Figure 5a). The cure temperature was maintained at 130 °C, and various FTIR spectra were obtained to understand the progression of the curing process. Consequently, the two bands associated with the symmetric and asymmetric epoxy ring deformation at 821 cm^{-1} and 844 cm^{-1} were monitored over time (Figure 5b,c).

After UV curing, both polymers exhibited a decrease in these bands, indicating that the S_N2 reaction can occur during photopolymerization due to the heat release associated with radical chain growth. Interestingly, the MAGSO-C reached an epoxy conversion of 57 ± 8% just after the photopolymerization process, which is higher than that observed for MAGSO-G (17 ± 2%). This can be attributed to the hydroxyl groups present in the ricinoleic fatty chain, which can attack the epoxy rings to form ether groups.[36,118] However, since MAGSO-G does not contain ricinoleic chains, the conversion may also be due to the attack of carboxylic acids on the epoxy groups.[30,36]

After 30 min at 130 °C, both polymers exhibited similar epoxy conversion, reaching values of 74 ± 4% for MAGSO-G and 74 ± 6% for MAGSO-C. These polymers were cured for an additional 30 min, and the conversion reached 77 ± 1% (MAGSO-G) and 81 ± 6% (MAGSO-C). Thereafter, the polymers were maintained at this temperature for an additional 4 h, and at each hour, the conversion of the epoxy group was monitored. Therefore, after 120 min, the MAGSO-G achieved a conversion of 85 ± 4% and the MAGSO-C reached a conversion of 89 ± 4%. The maximum conversion was achieved after a total of 180 min (3 h). Then, the MAGSO-G presented a conversion of 91 ± 2%, and the MAGSO-C a conversion of 91 ± 2%. After that, the conversion remained constant for the next 2 h. For MAGSO-G, the conversion was 91 ± 2% (240 min) and 92 ± 1% (300 min), and for MAGSO-C, it was 91 ± 1% (240 min) and 93 ± 1% (300 min). These findings presented that the dual-cure is viable in just 3 h at a midtemperature, and the total conversion was higher than 90%.

Cross-linked polymeric materials produced by UV curing and after thermal curing were subjected to gel content (GC, Figure 6a) in order to verify the incorporation of monomers into the final polymeric matrix. Higher GC indicates a lower remaining monomer amount and can also be linked to the conversion of each material.[28] Polymeric materials immediately after UV curing (MAGSO-B, MAGSO-C, and MAGSO-G) exhibited GC values of 95.5 ± 0.5%, 98.8 ± 0.7%, and 96.7 ± 0.6%, respectively. Although the conversion by FTIR and DSC only exhibited conversions of around 40%, the GC value indicates that at least one functional methacrylic pendant was reacted to and participates in the network. Furthermore, epoxy conversion by UV curing can contribute to higher GC. As expected, polymers after thermal curing (MAGSO-CT and MAGSO-GT) exhibited an improvement in GC values, at 98.6 ± 0.4% and 98.87 ± 0.8%, respectively. Furthermore, the dual curing process is necessary to create hydroxyl groups (in the case of MAGSO-G) within the polymeric structure through epoxy ring opening after the S_N2 reaction. The hydroxyl in this system participates in the transesterification process and contributes to the self-healing feature.[35,100,119]

The tensiometric analysis yields contact angle values, indicating hydrophobic (≥90°) or hydrophilic (≤90°) properties.[28,46] The UV-cured polymers MAGSO-B, MAGSO-C, and MAGSO-G presented values of 87 ± 1°, 54 ± 1°, and 89 ± 1°, respectively (Figure 6b). MAGSO-B and MAGSO-C presented angle values close to a hydrophobic material; in contrast, MAGSO-C presented a hydrophilic feature, which can be related to hydroxyl groups from ricinoleic fatty chains. In fact, castor oil is more hydrophilic than other vegetable oils, being able to have a better emulsion effect with water and other polar compounds such as thiols.[46] After thermal curing, the MAGSO-CT continued to exhibit the hydrophilic characteristic (61 ± 1°), while the MAGSO-GT decreased the angle value, also presenting as a hydrophilic material (72 ± 1°). This hydrophilic aspect is expected to increase after thermal curing since more polar groups are present in the polymeric network. These results suggest that the polymers can be tailored to meet the specific needs of various applications. All GC and tensiometric values are presented in Table 3.

A hydrolysis test was also conducted for each polymer at room temperature using a sodium hydroxide solution (1.0 mol L^{-1}) for 48 h. Photographs were taken to document the progress of degradation (Figure 6c). At the initial time (t = 0), no degradation was observed. However, after 2 h, the samples MAGSO-B, -C, and -G exhibited an advanced degradation process with remaining polymeric matrices; in contrast, the

https://doi.org/10.1021/acssuschemeng.5c07154
ACS Sustainable Chem. Eng. 2025, 13, 16136−16153

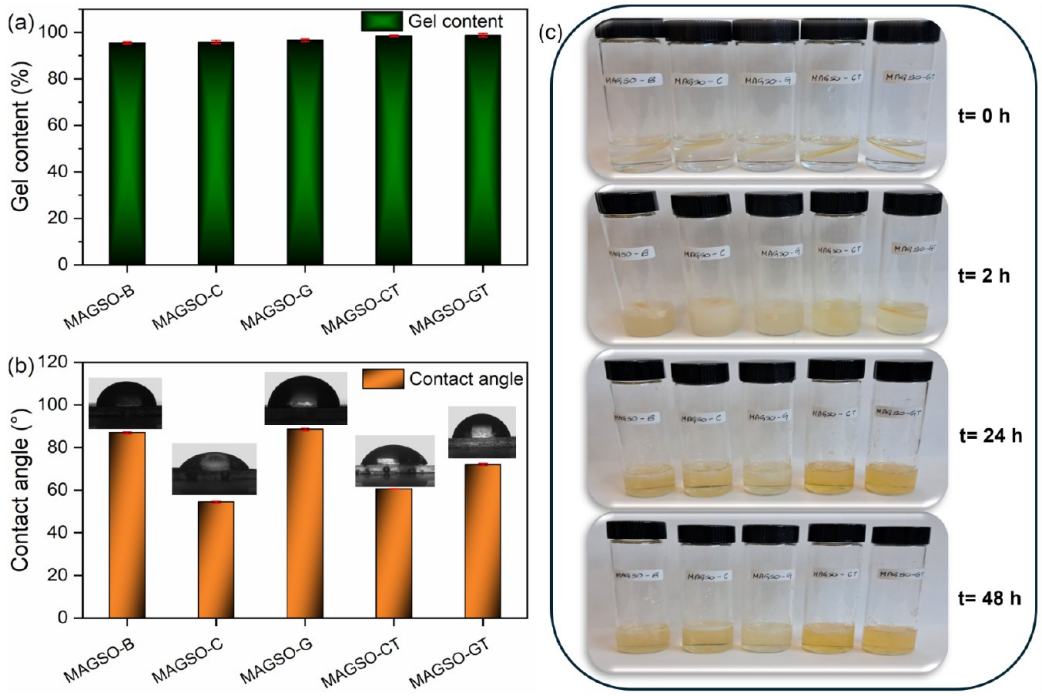

Figure 6. (a) gel content, (b) contact angle, and (c) hydrolysis test for each polymer.

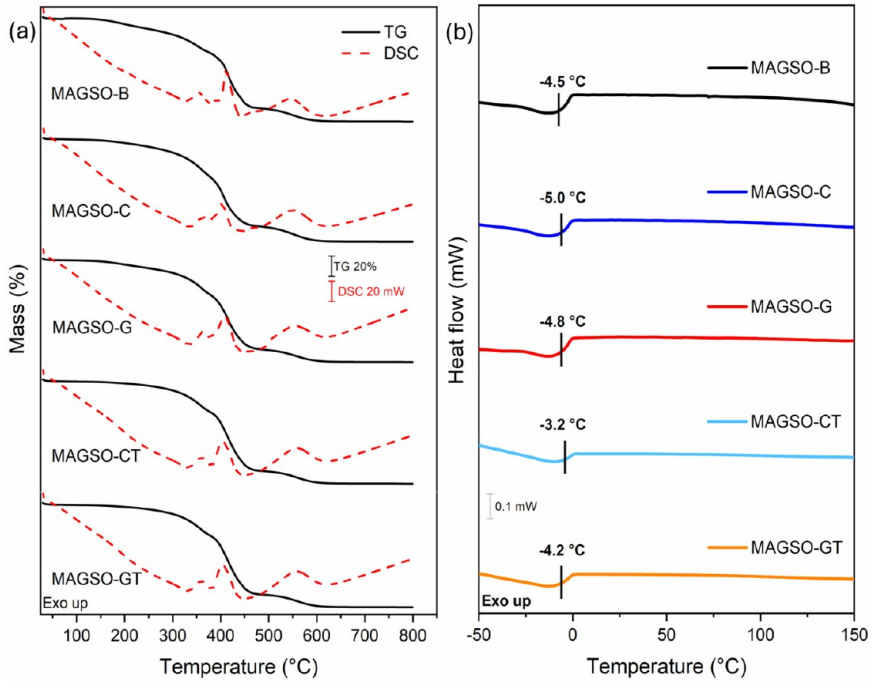

Figure 7. (a) TG/DSC curves, (b) DSC curves for each UV-cured and UV/thermal-cured sample.

MAGSO-CT and -GT showed a lower degree of degradation. After 24 h, all UV-cured samples without thermal treatment were completely degraded, leaving only a fine white powder associated with the methacrylated polymeric matrices and a yellowish solution; however, the thermally cured polymers still displayed a visible network structure. Lastly, after 48 h, all polymeric matrices were degraded, and the presence of a white powder and a yellow solution was noted. This study is important because hydrolysis can be related to the ability to chemically degrade polymers at the end of their life, thereby preventing them from accumulating in the environment.[25,27,30,31]

Thermal Properties, Thermal Reprocessing, and Chemical Recyclability. Thermogravimetric curves for all photocurable formulations, excluding epoxy monomer (MAGSO-B), and featuring epoxy monomer prior to thermal curing (MAGSO-C, -G), and post-thermal curing (MAGSO-CT, -GT) are presented in Figure 7a. Two main stages of mass loss are observed for these polymers, indicating similar thermal degradation profiles, except for the thermal stability temperature ($T_{stability}$), which signifies the maximum temperature the

https://doi.org/10.1021/acssuschemeng.5c07154
ACS Sustainable Chem. Eng. 2025, 13, 16136−16153

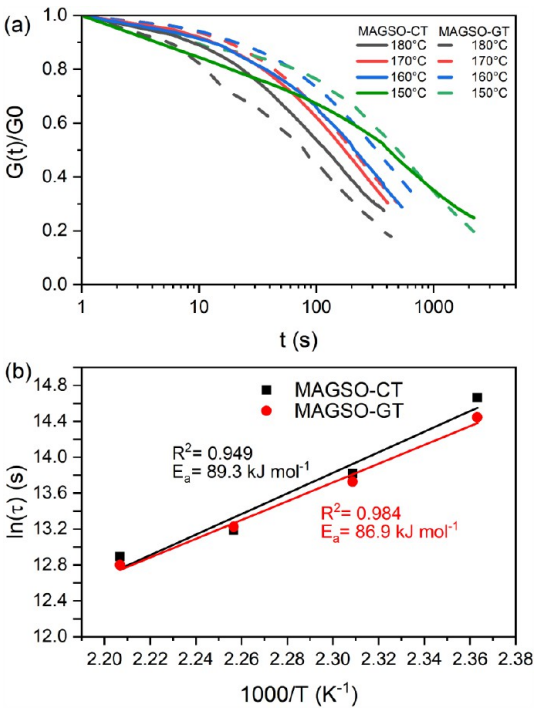

Figure 8. (a) stress relaxation $G(t)/G_0$ curves for MAGSO-CT (solid line) and MAGSO-GT (dashed line), and (b) linear fitting curves calculated by the Arrhenius equation and activation energy for MAGSO-CT and MAGSO-GT.

samples can endure before degradation begins. MAGSO-B exhibits the lowest $T_{stability}$ at 150 °C, while incorporating the epoxy monomer increases this temperature to 200 °C. After thermal curing, these polymers can withstand temperatures as high as 220 °C. The first decomposition stage corresponds to the degradation of the polymeric network, while the second stage involves the decomposition and combustion of carbonaceous matter in the presence of oxygen.[29,31] Furthermore, exothermic events are observed at all stages of mass loss in the DSC curve. Detailed properties related to the TGA/DSC curves are outlined in Table S1.

The DSC curves displayed in Figure 7b correspond to the heating stage (−50−150 °C) and show the glass transition temperature (T_g) for all samples. It is noted that all samples presented a T_g between −3.0 °C and −5.0 °C, which is consistent with the T_g values reported for other vegetable oil-based polymers in the literature. This relatively low T_g is attributed to the longer fatty chains in the triacylglycerol structure.[29,31] Consequently, all polymers are in a rubbery state at room temperature (25 °C).

The stress-relaxation curves for UV-thermal cured MAGSO-CT and MAGSO-GT are presented in Figure 8a. TG curves determined the temperature for this study, as the polymer cannot degrade during the stress-relaxation experiment. Therefore, stress-relaxation curves were recorded at four different temperatures: 150 °C, 160 °C, 170 °C, and 180 °C.

For both materials, as the temperature increases, the relaxation modulus decays more rapidly, indicating a faster relaxation behavior.

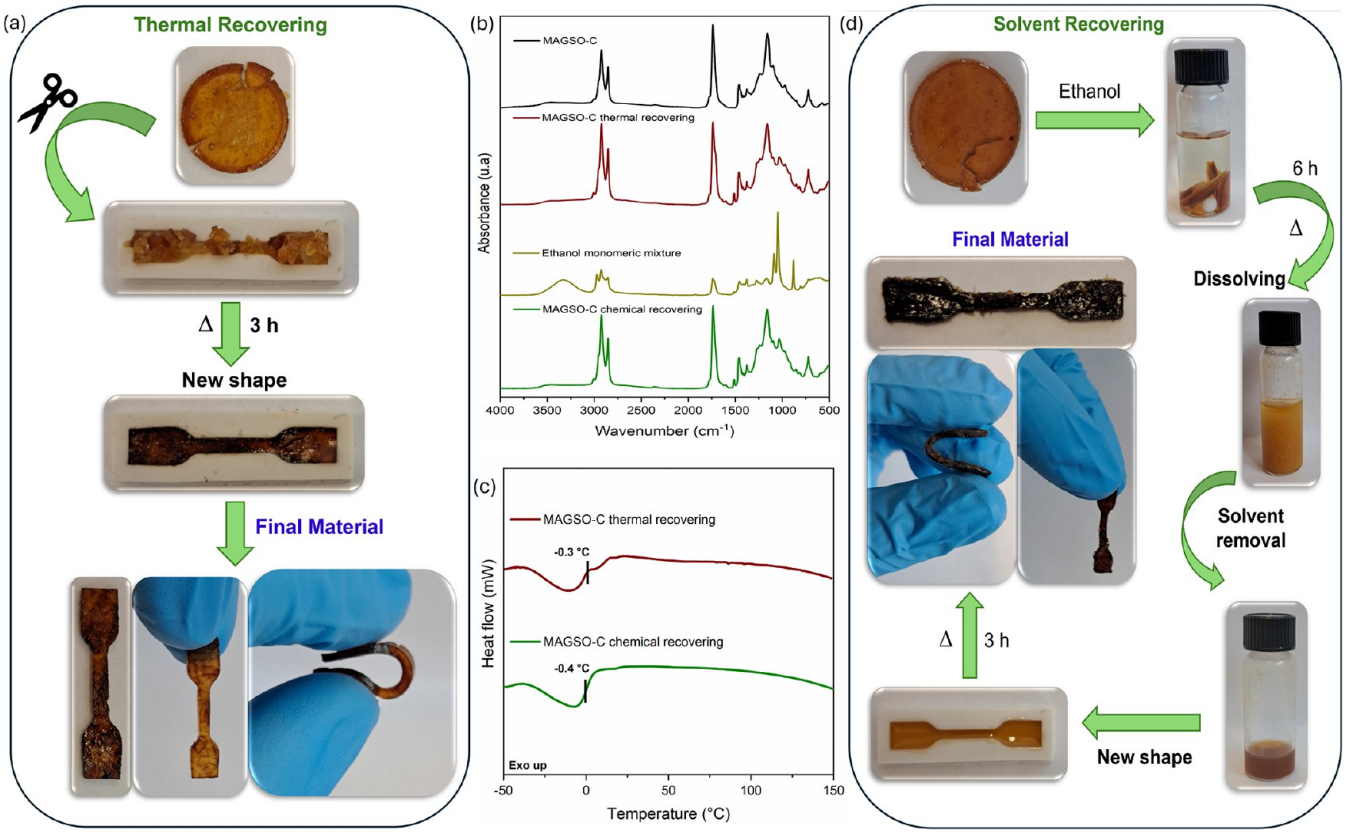

Figure 9. (a) Thermal recovering at 150 °C for 3 h, (b) FTIR of MAGSO-C before thermal recovering, after thermal recovering, ethanol monomeric mixture, and MAGSO-C after chemical recovering, (c) DSC curves for MAGSO-C after thermal and chemical recovering, and (d) solvent recovering using ethanol as transesterification agent and polymer after chemical recovery.

https://doi.org/10.1021/acssuschemeng.5c07154
ACS Sustainable Chem. Eng. 2025, 13, 16136−16153

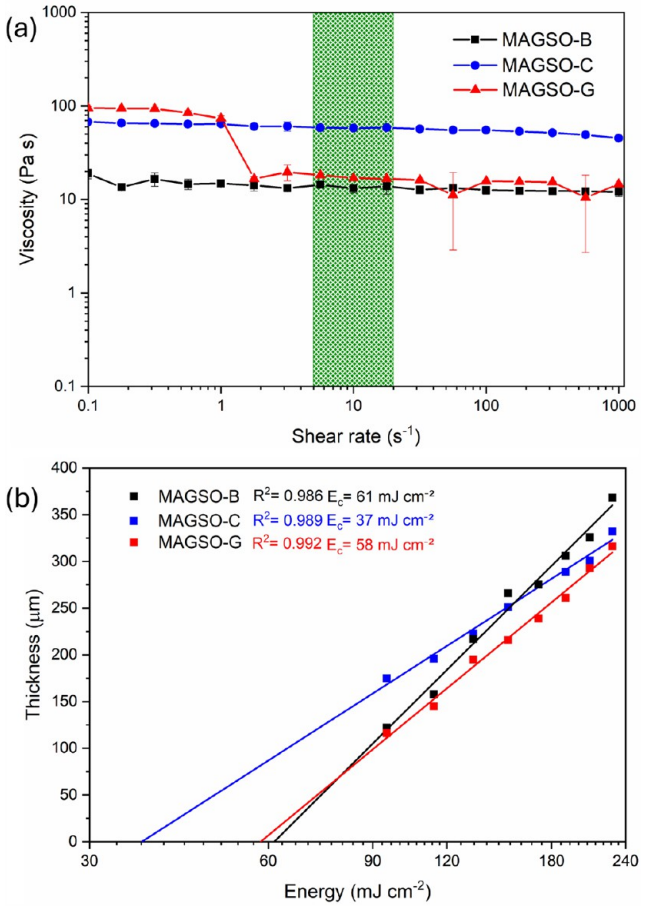

Figure 10. (a) Viscosity measurements and (b) working curves and critical energy for each photocurable formulation.

The relaxation curves do not appear Debye-like in Figure 8a. Therefore, to calculate E_a, we used the Kohlrausch−Williams−Watts (KWW) model (including an elastic offset G∞). From these fits, we obtained, for each temperature, the characteristic time τ (used in the Arrhenius plot) and the shape parameter β, which reflects the breadth of the relaxation-time spectrum and, operationally, the degree of network homogeneity. In the KWW equation, β =1 denotes a Debye-like, narrow spectrum (effectively a single dominant process). In contrast, a smaller β indicates a broader distribution (greater heterogeneity), which can be attributed to different polymeric matrices or competitive associative and dissociative reactions.[101−103] For the MAGSO-CT, the β value was 0.98, which is close to a Debye-like curve. From this, the E_a, was calculated, yielding a value of 89.3 kJ mol^{-1}. For the MAGSO-GT, the β value was 0.84, indicating a more heterogeneous system with E_a, of 86.9 kJ mol^{-1} (Figure 8b).

The activation energies from both systems are similar, as expected, since the chemical structures of the monomers are alike. The 0.2 difference in the β value might result from different chemical processes during relaxation. The main process is an associative reaction catalyzed by the EUPG (Brønsted-Lowry acid catalyst). Therefore, the ester groups become protonated and can react with alcohol groups in the polymer matrix, leading to transesterification. The MAGSO-CT has more alcohol groups (−OH) in the matrix because of the ricinoleic fatty chain, which enhances the transesterification process (nucleophilic acyl substitution).[120,121] This suggests a β-value of 0.98 and a primarily associative reaction. In contrast, MAGSO-GT has fewer alcohol groups, only those formed from epoxy ring opening after thermal curing. Therefore, a dissociative process may then occur, involving cyclization of the ester group next to the carboxylic acid, forming an intermediate anhydride.[122] This group is attacked by the alcohol (nucleophile), resulting in the formation of a new ester. In both cases, the final product is an ester, but the steps differ, which could influence the heterogeneity and the β value.[122]

Subsequently, the samples used in the stress-relaxation analysis were also employed to investigate the self-healing process, as both MAGSO-CT and -GT exhibited dynamic covalent network properties that could be exploited in self-healing behavior. The final material (thermally recovered) exhibited an FTIR spectrum similar to that of the original sample (Figure 9b) and a T_g of −0.3 °C, as determined by DSC (Figure 9c). These results confirm the self-healing ability of this material.

The solvent recovery process (Figure 9d) was also conducted using ethanol as the transesterification agent. This ethanol-based monomeric solution has an orange color, a gel-like appearance, and a sticky aspect. FTIR analysis of the material revealed that the spectrum (Figure 9b) showed a significant reduction in the band at 1741 cm^{-1}, associated with C═O stretching in ester groups, indicating breakdown of the polymeric network. Additionally, the band at 3328 cm^{-1} corresponds to the O−H stretching of residual ethanol.

This monomeric mixture was then poured into the silicon mold (dogbone shape) and subsequently cured in the same process as aforementioned. The recovered polymeric material presents a darker color than the original material, but it was tack-free, presenting a complete cure. The final polymer was then characterized by FTIR and presented a similar spectrum to the original MAGSO-CT; therefore, the band related to C═O stretching at 1741 cm^{-1} was completely recovered, and the band at 3328 cm^{-1} for O−H stretching was diminished due to the removal of ethanol. The recovered polymeric materials presented a T_g at 0.4 °C (Figure 9c). These results confirmed the recovery process and self-healing capability using the chemical/solvent process. These results open new possibilities for applications in adhesives, coatings, and self-healing materials.[100,119]

Furthermore, green design was essential for producing renewable materials with self-healing features, as the polymer was designed to contain a high quantity of ester and hydroxyl groups. This recovery process is aligned with the Green Chemistry and mainly with the Circular Economy (recycling/recovering materials).

3D Printing. For good printability, the photocurable formulations should remain within an ideal viscosity range, referred to as the printability range. This range is between 0.2 Pa·s and 10.0 Pa·s for viscosity, while the shear rate is between 5 s^{-1} and 20 s^{-1}.[28,46,60,106,123] This ensures a proper flow of this formulation in the VAT, which enhances homogeneity and printability layer by layer.

Therefore, the MAGSO-B, -C, and -G were measured using a parallel plate geometry rheometer to determine their viscosities (Figure 10a). None of the photocurable formulations presented an ideal viscosity range (indicated by the green square). The MAGSO-B and MAGSO-G presented viscosities close to the necessary range at a shear rate of 10 s^{-1} (13.1 ± 1.4 Pa·s and 16.9 ± 0.8 Pa·s, respectively). The MAGSO-C presented a higher viscosity at the same shear rate (57.8 ± 2.0

https://doi.org/10.1021/acssuschemeng.5c07154
ACS Sustainable Chem. Eng. 2025, 13, 16136−16153

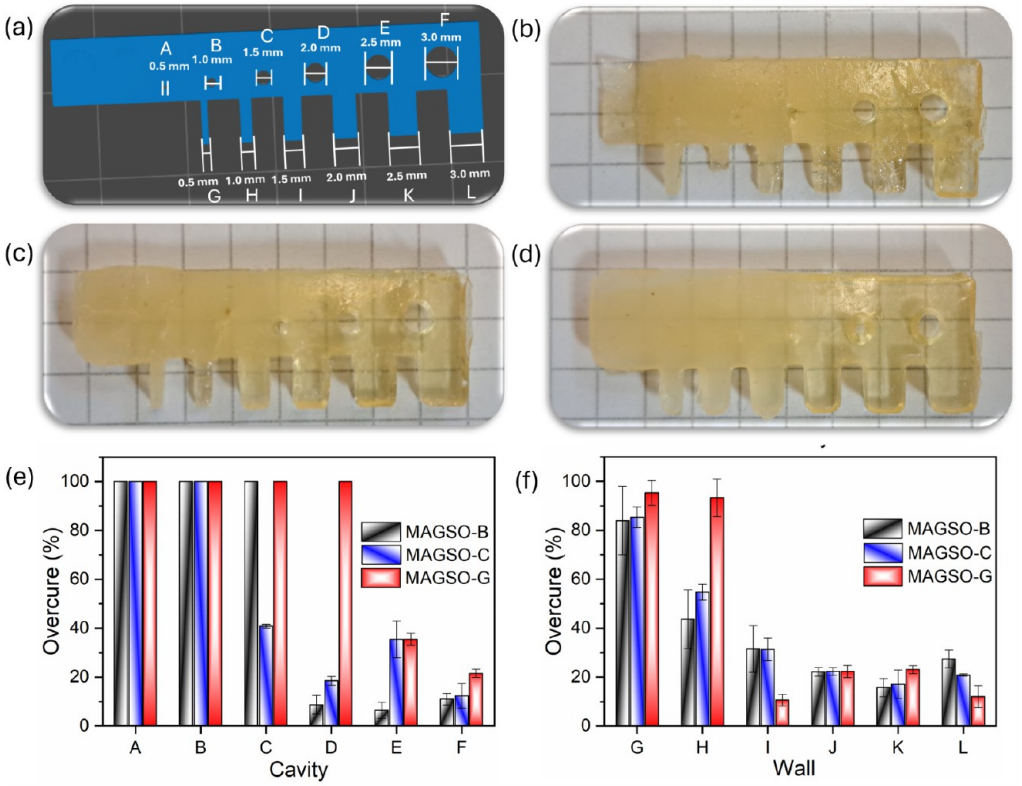

Figure 11. (a) CAD model for overcuring evaluation, (b) MAGSO-B, (c) MAGSO-C, (d) MAGSO-G, (e) overcure percentage considering the cavity, and (f) overcure percentage considering the wall.

Pa·s). However, all photocurable formulation had their critical energy determined by the working curves and were tested in the 3D printer.

Critical energy (E_c) is the amount of energy required to initiate the gelation process in monomeric formulations. After a certain exposure time, the thickness of the resulting film is measured and correlated with the energy of the light source. This allows for the creation of a curve plotting energy against thickness at each time point (Figure 10b). All epoxy monomeric mixtures were tested over a range of times from 50 to 120 s.

At the shortest exposure time (50 s), the trend was: **MAGSO-C (175 μm) > MAGSO-G (116 μm) > MAGSO-B (122 μm)**. This indicates that epoxy castor oil enhances film formation in a shorter time. This improvement can be attributed to the increased molecular interaction between monomers, resulting from the presence of hydroxyl groups.[46] However, when the exposure time exceeds 80 s, the MAGSO-B system produces a thicker film than the epoxy system, allowing for greater light penetration. At 120 s, the trend is **MAGSO-B (266 μm) > MAGSO-C (251 μm) > MAGSO-G (216 μm)**. Throughout the process, MAGSO-C exhibited a more efficient polymerization process, resulting in a lower E_c (37 mJ cm^{-2}), followed by MAGSO-G (58 mJ cm^{-2}), and finally MAGSO-B (61 mJ cm^{-2}).

Based on the working curves and critical energy values, the exposure time for each layer was set to 80 s, while the bottom layer was exposed for 120 s. The formulations were printed in a comb shape to evaluate the overcuring process; therefore, cavities with different diameters and walls with varying widths are present in this structure (Figure 11a). The difference between the theoretical structure (printer file, Figure 11a) and the experimental objects can provide insights into the overcuring process. The MAGSO-B (Figure 11b) experienced total overcuring in the first three cavities (0.5 mm to 1.5 mm). For the remaining cavities, the overcuring range was reduced to 20% to 40%, and an overcuring of 80% was observed in the first wall.

The MAGSO-C showed overcuring for the first two cavities and about 80% overcuring for the first wall (Figure 11c); however, this system had the lowest overcuring among all. In contrast, the MAGSO-G (Figure 11d) exhibited a higher overcuring process, as the first four cavities were completely overcured, and the first two walls had overcuring rates exceeding 90%. The overcuring processes for cavities and walls are shown in Figure 11e,f, respectively, and the measurement and overcuring values are listed in Table S2.

All photocurable formulations were tested using the 3D printer; therefore, the honeycomb structures for each sample are shown in Figure 12a. The printed structure measured 10 mm in width and 1 mm in height, enabling resolution studies. As expected, the MAGSO-G showed overcuring since the cavities are closer; however, the MAGSO-B and MAGSO-C demonstrated good resolutions.

The MAGSO-C was also used to print a net with a width of 25 mm and a height of 1.0 mm to ensure flexibility (Figure 12b). Then, the net was thermally cured (3 h at 130 °C) in a bent shape to determine if it can maintain its form after cooling. As expected, thermal curing increases the network regidity,[78,119] enabling the polymer to retain a permanent bent shape. The ability to program the final shape through thermal curing expands the functional scope of photocurable biobased resins toward sustainable manufacturing. Furthermore, an octopus structure (Figure 12c) was also printed to

https://doi.org/10.1021/acssuschemeng.5c07154
ACS Sustainable Chem. Eng. 2025, 13, 16136−16153

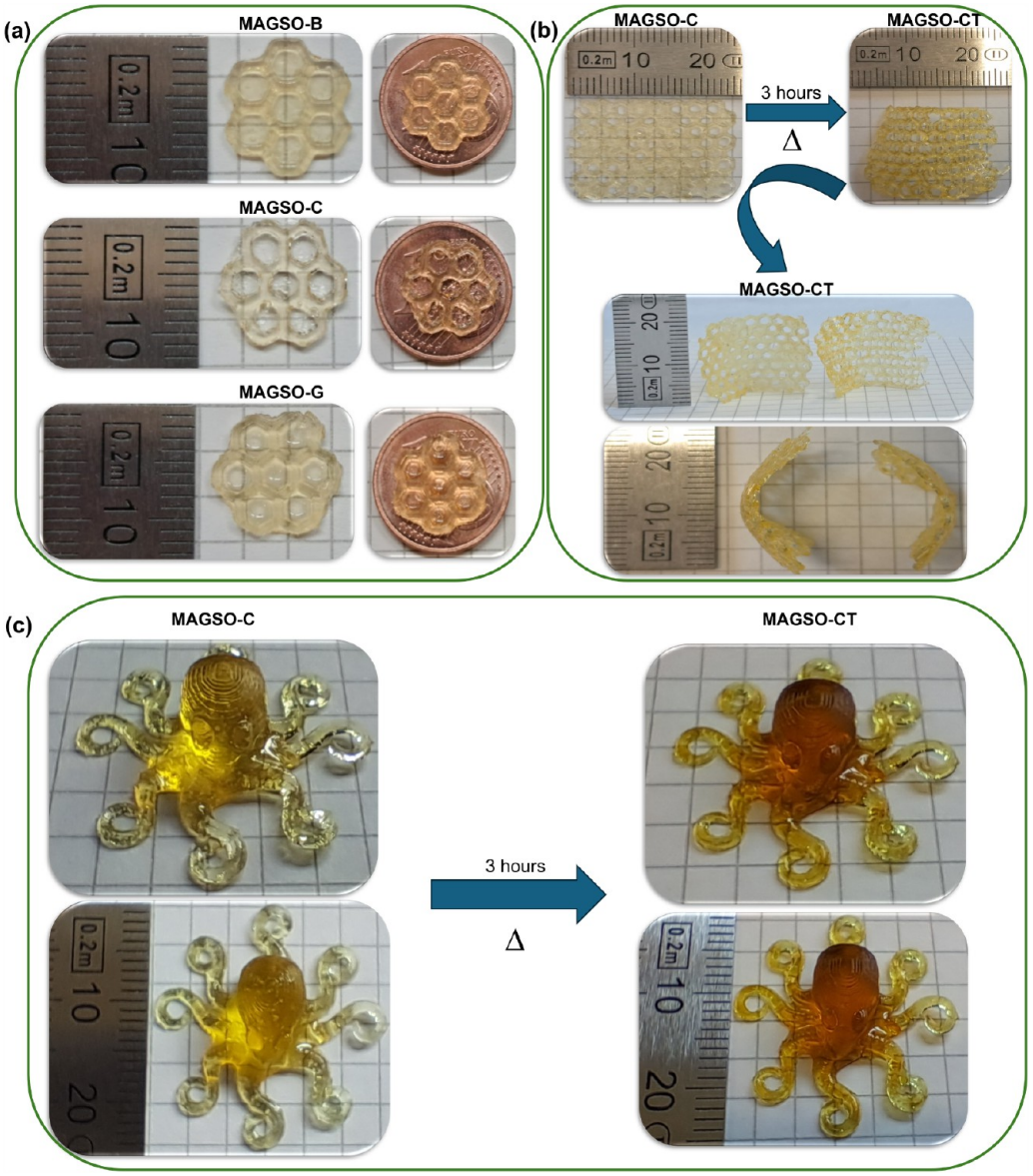

Figure 12. (a) 3D-printed honeycomb structures for some of the photocurable formulations, (b) thermal curing test for fixed shape, and (c) bulk structure with detailed features (octopus).

Table 2. FTIR and DSC Results Regarding Conversion (%), Enthalpy, and Rate of Polymerization (R_p) for Each Photocurable Formulation Resin

	FTIR			DSC		
Sample	C (%)	R_p (s^{-1})	Peak time (s)	ΔH ($J\ g^{-1}$)	C (%)	R_p (s^{-1})
MAGSO-B	42 ± 2	0.022	5	39.6	41	0.026
MAGSO-C	57 ± 3	0.038	5	34.6	36	0.020
MAGSO-G	41 ± 1	0.032	5	36.0	37	0.022

demonstrate the ability to print large structures with detailed features.

CONCLUSIONS

This study introduces a new class of polymers that combines a dual-curing process and covalent dynamic networks—CANs into a single system made entirely from vegetable oils through a green design approach. The resulting materials are not only reprocessable and chemically recyclable but also degradable under mild alkaline conditions, meeting key requirements for a circular economy.

Polymers demonstrate self-healing behavior through transesterification, and these formulations are compatible with 3D printing technologies. Although formulations exceeded ideal viscosities and experienced overcuring in some points, they effectively produced well-defined printed structures, confirming the feasibility of using CANs renewable/biobased resins in additive manufacturing.

Overall, this work advances the development of fully biobased, closed-loop polymer systems that combine functionality and sustainability. Future efforts will focus on the mechanical properties of high-performance structures, as well as exploring the use of reprocessable and chemically recyclable materials with potential applications in coatings and adhesives.

https://doi.org/10.1021/acssuschemeng.5c07154
ACS Sustainable Chem. Eng. 2025, 13, 16136−16153

Table 3. Physical-Chemical Properties of All Photocurable Formulations and Polymers

	MAGSO-B	MAGSO-C	MAGSO-G	MAGSO-CT	MAGSO-GT
BC (%)	98.0	85.3	85.3	85.3	85.3
BCC (%)	63.1	72.6	72.6	72.6	72.6
GC (%)	95.5 ± 0.5%	95.8 ± 0.7%	96.7 ± 0.6%	98.6 ± 0.4%	98.8 ± 0.8%
Contact angle (°)	87 ± 1	54 ± 1	89 ± 1	61 ± 1	72 ± 1
$T_{stability}$-TG (°C)	150	200	200	220	220
T_g-DSC (°C)	−4.5	−5.0	−4.8	−3.2	−4.2
Viscosity at 10 s^{-1} (Pa·s)	13.1 ± 1.4	16.9 ± 0.8	57.8 ± 2.0	-	-
Critical energy (mJ cm^{-2})	61	37	58	-	-

■ ASSOCIATED CONTENT

Data Availability Statement

Authors can confirm that all relevant data are included in the article.

Supporting Information

The Supporting Information is available free of charge at https://pubs.acs.org/doi/10.1021/acssuschemeng.5c07154.

^{1}H NMR and FTIR spectra for vegetable oils and functionalized derivatives; table containing events of TG curves; and table containing events measurements of the comb-shaped test structures (PDF)

■ AUTHOR INFORMATION

Corresponding Authors

Rafael T. Alarcon − *Universidade de São Paulo-USP, Instituto de Química de São Carlos, São Carlos, São Paulo 13566-590, Brazil;* orcid.org/0000-0003-2798-9587; Email: rafael.alarcon@usp.br

Marco Sangermano − *Dipartimento Scienza Applicata e Tecnologia, Politecnico di Torino, Torino 10129, Italy;* orcid.org/0000-0002-8630-1802; Email: marco.sangermano@polito.it

Authors

Alberto Cellai − *Dipartimento Scienza Applicata e Tecnologia, Politecnico di Torino, Torino 10129, Italy;* orcid.org/0009-0008-7543-036X

Matilde Porcarello − *Dipartimento Scienza Applicata e Tecnologia, Politecnico di Torino, Torino 10129, Italy*

Bernhard Sölle − *Polymer Competence Center Leoben GmbH (PCCL), Leoben 8700, Austria*

Elisabeth Rossegger − *Polymer Competence Center Leoben GmbH (PCCL), Leoben 8700, Austria;* orcid.org/0000-0003-4924-1262

Carla C. Schmitt − *Universidade de São Paulo-USP, Instituto de Química de São Carlos, São Carlos, São Paulo 13566-590, Brazil;* orcid.org/0000-0001-9952-4741

Complete contact information is available at: https://pubs.acs.org/10.1021/acssuschemeng.5c07154

Author Contributions

The manuscript was written with contributions from all authors. All authors have approved the final version of the manuscript.

Funding

The Article Processing Charge for the publication of this research was funded by the Coordenacao de Aperfeicoamento de Pessoal de Nivel Superior (CAPES), Brazil (ROR identifier: 00x0ma614).

Notes

The authors declare no competing financial interest.

■ ACKNOWLEDGMENTS

The authors thank the São Paulo Research Foundation (FAPESP) for financial support (grants: 2024/03936-1 and 2021/14879-0).

■ REFERENCES

(1) King, O.; Pérez-Madrigal, M. M.; Murphy, E. R.; Hmayed, A. A. R.; Dove, A. P.; Weems, A. C. 4D Printable Salicylic Acid Photopolymers for Sustained Drug Releasing, Shape Memory, Soft Tissue Scaffolds. *Biomacromolecules* **2023**, *24*, 4680−4694.

(2) Aguirre, M.; Hamzehlou, S.; González, E.; Leiza, J. R. Renewable Feedstocks in Emulsion Polymerization: coating and Adhesive Applications. In *Advances in Chemical Engineering*; Academic Press, 2020; Vol. *56*, DOI: .

(3) Bailón-Moreno, R.; Romero-Noguera, J.; Bolívar-Galiano, F. C.; Yebra-Rodríguez, A. M.; Pérez-Villares, N. Response Surfaces Model for Restoring and Cleaning Oil Painted Artworks. *J. Cult. Herit.* **2020**, *45*, 10−24.

(4) Wei, S.; Li, Z.; Lu, W.; Liu, H.; Zhang, J.; Chen, T.; Tang, B. Z. Multicolor Fluorescent Polymeric Hydrogels. *Angew. Chem., Int. Ed.* **2021**, *60* (16), 8608−8624.

(5) Nam, S.; Mooney, D. Polymeric Tissue Adhesives. *Chem. Rev.* **2021**, *121* (18), 11336−11384.

(6) Chiarioni, G.; van Duin, M.; Pescarmona, P. P. Novel Elastic Rubbers from CO2-Based Polycarbonates. *Green Chem.* **2023**, *25* (19), 7612−7626.

(7) Bergoglio, M.; Palazzo, G.; Reisinger, D.; Porcarello, M.; Kortaberria, G.; Schlögl, S.; Sangermano, M. Cationic UV-Curing of Bio-Based Epoxidized Castor Oil Vitrimers with Electrically Conductive Properties. *React. Funct. Polym.* **2024**, *200*, 105936.

(8) Amukarimi, S.; Rezvani, Z.; Eghtesadi, N.; Mozafari, M. Smart Biomaterials: From 3D Printing to 4D Bioprinting. *Methods* **2022**, *205*, 191−199.

(9) Alarcon, R. T.; Gaglieri, C.; dos Santos, G. C.; Moralles, A. C.; Morgon, N. H.; de Souza, A. R.; Bannach, G. AIE Effect by Oxygen Clustering in Vegetable Oil-Based Polymers. *ChemistrySelect* **2021**, *6* (31), 7838−7844.

(10) da Silva, R.; Alarcon, R. T.; Cavalheiro, É. T. G. Determination of Sildenafil in Pharmaceutical Formulations and Synthetic Urine Using a Composite Electrode Composed of Acetylene Black Modified with Silver Nanoparticles and Vegetable Oil-Derived Polyurethane. *J. Electroanal. Chem.* **2025**, *979*, 118938.

(11) PlasticsEurope. *Plastics − the fast facts 2023*; 2023. https://plasticseurope.org/knowledge-hub/plastics-the-fast-facts-2023/. (accessed 15 July 2025).

(12) Sardon, H.; Dove, A. P. Plastics Recycling with a Difference. *Science* **2018**, *360*, 380−381.

(13) Kümmerer, K.; Clark, J. H.; Zuin, V. G. Rethinking Chemistry for a Circular Economy. *Science* **2020**, *367* (6476), 369−370.

(14) Szekely, G. The 12 Principles of Green Membrane Materials and Processes for Realizing the United Nations' Sustainable Development Goals. *RSC Sustainability* **2024**, *2* (4), 871−880.

(15) Zuin, V. G.; Kümmerer, K. Chemistry and Materials Science for a Sustainable Circular Polymeric Economy. *Nat. Rev. Mater.* **2022**, *7* (2), 76−78.
(16) Walker, T. R. (Micro)Plastics and the UN Sustainable Development Goals. *Curr. Opin. Green Sustainable Chem.* **2021**, *30*, 100497.
(17) Tarazona, N. A.; Machatschek, R.; Balcucho, J.; Castro-Mayorga, J. L.; Saldarriaga, J. F.; Lendlein, A. Opportunities and Challenges for Integrating the Development of Sustainable Polymer Materials within an International Circular (Bio)Economy Concept. *MRS Energy Sustain.* **2022**, *9* (1), 28−34.
(18) Geyer, R.; Jambeck, J. R.; Law, K. L. P. Use, and Fate of All Plastics Ever Made. *Sci. Adv.* **2017**, *3* (7), 25−29.
(19) Sheldon, R. A.; Norton, M. Green Chemistry and the Plastic Pollution Challenge: Towards a Circular Economy. *Green Chem.* **2020**, *22* (19), 6310−6322.
(20) Gracida-Alvarez, U. R.; Xu, H.; Benavides, P. T.; Wang, M.; Hawkins, T. R. Circular Economy Sustainability Analysis Framework for Plastics: Application for Poly(Ethylene Terephthalate) (PET). *ACS Sustainable Chem. Eng.* **2023**, *11* (2), 514−524.
(21) Ncube, A.; Mtetwa, S.; Bukhari, M.; Fiorentino, G.; Passaro, R. Circular Economy and Green Chemistry: The Need for Radical Innovative Approaches in the Design for New Products. *Energies* **2023**, *16* (4), 1752.
(22) Kurul, F.; Doruk, B.; Topkaya, S. N. Principles of Green Chemistry: Building a Sustainable Future. *Discov. Chem.* **2025**, *2* (1), 68.
(23) Ramirez-Corredores, M. M. Sustainable Production of CO_2-Derived Materials. *Mater. Sustainability* **2024**, *2*, 35.
(24) Chyr, G.; DeSimone, J. M. Review of High-Performance Sustainable Polymers in Additive Manufacturing. *Green Chem.* **2023**, *25* (2), 453−466.
(25) Cheng, H. N.; Gross, R. A.; Smith, P. B.Green Polymer Chemistry: Pipelines toward New Products and Processes*Green Polymer Chemistry: new Products, Processes, and Applications*ACS Publications2018Vol. *1310*pp. 1−11
(26) Sternberg, J.; Sequerth, O.; Pilla, S. Green Chemistry Design in Polymers Derived from Lignin: Review and Perspective. *Prog. Polym. Sci.* **2021**, *113*, 101344.
(27) Kerton, F. M. Applying the Principles of Green Chemistry to Achieve a More Sustainable Polymer Life Cycle. *Curr. Opin. Green Sustainable Chem.* **2025**, *51*, 100996.
(28) Alarcon, R. T.; Cellai, A.; Schmitt, C. C.; Gomes Cavalheiro, É. T.; Sangermano, M. Ternary Formulations of Bio-Based Grapeseed Oil-Based Monomers for 3D Printing: Effect of Thiol-Ene Reaction on Acrylic Radical Photopolymerization. *Eur. Polym. J.* **2025**, *235*, 114068.
(29) Alarcon, R. T.; Gaglieri, C.; de Freitas, J.; Bannach, G.; Cavalheiro, É. T. G. Synthesis and Characterization of Self-Healing Polymers Obtained from Polyphenols and Cyclic Carbonates of Amide Derivative of Macaw Palm Oil. *J. Polym. Environ.* **2025**, *33*, 1159−1170.
(30) Vermiglio, A. L.; Alarcon, R. T.; Cavalheiro, É. T. G.; Bannach, G.; Farmer, T. J.; North, M. Highly Crosslinked Polyesters Prepared by Ring-Opening Copolymerization of Epoxidized Baru Nut and Macaw Palm Oils with Cyclic Anhydrides. *RSC Sustainability* **2023**, *1* (4), 987−993.
(31) Alarcon, R. T.; Gaglieri, C.; Bannach, G.; Cavalheiro, É. T. G. Greener Preparation of a Flexible Material Based on Macaw Palm Oil Derivatives and CO2. *Green Chem.* **2024**, *26* (6), 3261−3270.
(32) Alarcon, R. T.; dos Santos, G. I.; Gaglieri, C.; de Moura, A.; Cavalheiro, E. T. G.; Bannach, G. Lipidic Biomass as a Renewable Chemical Building Block for Polymeric Materials. *Chem. Commun.* **2024**, *60*, 14557−14572.
(33) Alarcon, R. T.; Porcarello, M.; Cellai, A.; Schmitt, C. C.; Sangermano, M. Advancing Green Additive Manufacturing: Epoxidized Vegetable Oils for Room-Temperature Photopolymerization 3D Printing. *Polymer* **2025**, *336*, 128868.
(34) Pires, O. A. B.; Alarcon, R. T.; Gaglieri, C.; da Silva-Filho, L. C.; Bannach, G. Synthesis and Characterization of a Biopolymer of Glycerol and Macadamia Oil. *J. Therm. Anal. Calorim.* **2019**, *137* (1), 161−170.
(35) Alarcon, R. T.; Lamb, K. J.; Cavalheiro, É. T. G.; North, M.; Bannach, G. A Screening Process for Carbonation of Vegetable Oils Using an Aluminum(Salen) Complex with a Further Application as Weldable Polymers. *J. Appl. Polym. Sci.* **2023**, *140* (24), No. e53962.
(36) Gaglieri, C.; Alarcon, R. T.; Magri, R.; North, M.; Bannach, G. Development of Renewable Thermosetting Polymers Based on Grape Seed Oil Derivatives. *J. Appl. Polym. Sci.* **2022**, *139* (41), No. e52990.
(37) Gaglieri, C.; Alarcon, R. T.; dos Santos, G. I.; Bannach, G. Renewable Disulfide-Based Polyesters: Highly Cross-Linked, Vitrimers, and Biodegradable Materials. *J. Therm. Anal. Calorim.* **2025**, *150* (9), 6697−6707.
(38) Pezzana, L.; Wolff, R.; Stampfl, J.; Liska, R.; Sangermano, M. High Temperature Vat Photopolymerization 3D Printing of Fully Bio-Based Composites: Green Vegetable Oil Epoxy Matrix & Bio-Derived Filler Powder. *Addit. Manuf.* **2024**, *79*, 103929.
(39) Mendes-Felipe, C.; Costa, P.; Roppolo, I.; Sangermano, M.; Lanceros-Mendez, S. Bio-Based Piezo- and Thermoresistive Photocurable Sensing Materials from Acrylated Epoxidized Soybean Oil. *Macromol. Mater. Eng.* **2022**, *307* (7), 2100934.
(40) Noè, C.; Malburet, S.; Bouvet-Marchand, A.; Graillot, A.; Loubat, C.; Sangermano, M. Cationic Photopolymerization of Bio-Renewable Epoxidized Monomers. *Prog. Org. Coat.* **2019**, *133*, 131−138.
(41) Mendes-Felipe, C.; Isusi, I.; Gómez-Jiménez-Aberasturi, O.; Prieto-Fernandez, S.; Ruiz-Rubio, L.; Sangermano, M.; Vilas-Vilela, J. L. One-Step Method for Direct Acrylation of Vegetable Oils: A Biobased Material for 3D Printing. *Polymers* **2023**, *15* (14), 3136.
(42) Bergoglio, M.; Reisinger, D.; Schlögl, S.; Griesser, T.; Sangermano, M. Sustainable Bio-Based UV-Cured Epoxy Vitrimer from Castor Oil. *Polymers* **2023**, *15* (4), 1024.
(43) Bergoglio, M.; Najmi, Z.; Cochis, A.; Miola, M.; Vernè, E.; Sangermano, M. UV-Cured Bio-Based Acrylated Soybean Oil Scaffold Reinforced with Bioactive Glasses. *Polymers* **2023**, *15* (20), 4089.
(44) Alarcon, R. T.; Lamb, K. J.; Bannach, G.; North, M. Opportunities for the Use of Brazilian Biomass to Produce Renewable Chemicals and Materials. *ChemSuschem* **2021**, *14* (1), 169−188.
(45) Gaglieri, C.; Alarcon, R. T.; De Moura, A.; Magri, R.; Da Silva-Filho, L. C.; Bannach, G. Green and Efficient Modification of Grape Seed Oil to Synthesize Renewable Monomers. *J. Braz. Chem. Soc.* **2021**, *32* (11), 2120−2131.
(46) Alarcon, R. T.; Bergoglio, M.; Cavalheiro, É. T. G.; Sangermano, M. Thiol-Ene Photopolymerization and 3D Printing of Non-Modified Castor Oil Containing Bio-Based Cellulosic Fillers. *Polymers* **2025**, *17* (5), 587.
(47) Alarcon, R. T.; Gaglieri, C.; de Souza, O. A.; Rinaldo, D.; Bannach, G. Microwave-Assisted Syntheses of Vegetable Oil-Based Monomer: A Cleaner, Faster, and More Energy Efficient Route. *J. Polym. Environ.* **2020**, *28* (4), 1265−1278.
(48) Mortier, J.; Stevens, C. V.; Heugebaert, T. S. A. Efficient Continuous Flow Oxidation of Furfural to Maleic Anhydride Using O_2 as a Green Oxidant. *Green Chem.* **2025**, *27*, 5063−5072.
(49) Cucciniello, R.; Cespi, D.; Riccardi, M.; Neri, E.; Passarini, F.; Pulselli, F. M. Maleic Anhydride from Bio-Based 1-Butanol and Furfural: A Life Cycle Assessment at the Pilot Scale. *Green Chem.* **2023**, *25* (15), 5922−5935.
(50) Li, X.; Ho, B.; Zhang, Y. Selective Aerobic Oxidation of Furfural to Maleic Anhydride with Heterogeneous Mo-V-O Catalysts. *Green Chem.* **2016**, *18* (10), 2976−2980.
(51) Müller, M.; Kutscherauer, M.; Böcklein, S.; Wehinger, G. D.; Turek, T.; Mestl, G. Modeling the Selective Oxidation of N-Butane to Maleic Anhydride: From Active Site to Industrial Reactor. *Catal. Today* **2022**, *387*, 82−106.
(52) Yu, T.; Zhang, J.; Yang, F.; Li, Q.; Chen, J.; Wang, G.; Wang, R. Vanadium Phosphorus Oxide Catalysts for n-Butane Selective

https://doi.org/10.1021/acssuschemeng.5c07154
ACS Sustainable Chem. Eng. 2025, 13, 16136−16153

Oxidation toward Maleic Anhydride: Design, Modification Strategies, and Progress. *Front. Chem. Sci. Eng.* **2025**, *19* (8), 65.
(53) Li, N.; Zong, M. H. (Chemo)Biocatalytic Upgrading of Biobased Furanic Platforms to Chemicals, Fuels, and Materials: A Comprehensive Review. *ACS Catal.* **2022**, *12* (16), 10080−10114.
(54) Li, X.; Zhang, Y. The Conversion of 5-Hydroxymethyl Furfural (HMF) to Maleic Anhydride with Vanadium-Based Heterogeneous Catalysts. *Green Chem.* **2016**, *18* (3), 643−647.
(55) Wu, Q.; Hu, Y.; Tang, J.; Zhang, J.; Wang, C.; Shang, Q.; Feng, G.; Liu, C.; Zhou, Y.; Lei, W. High-Performance Soybean-Oil-Based Epoxy Acrylate Resins: "Green" Synthesis and Application in UV-Curable Coatings. *ACS Sustainable Chem. Eng.* **2018**, *6* (7), 8340−8349.
(56) Zovi, O.; Lecamp, L.; Loutelier-Bourhis, C.; Lange, C. M.; Bunel, C. A Solventless Synthesis Process of New UV-Curable Materials Based on Linseed Oil. *Green Chem.* **2011**, *13* (4), 1014−1022.
(57) Yu, X.; Hu, Y.; Lei, W.; Liu, C.; Zhou, Y. Development of Catalyst-Free Self-Healing Biobased UV-Curable Coatings via Maleate Monoester Transesterification. *Coatings* **2023**, *13* (1), 110.
(58) Zhang, J.; Huang, J.; Zhu, G.; Yu, X.; Cheng, J.; Liu, Z.; Hu, Y.; Shang, Q.; Liu, C.; Hu, L.; Zhou, Y. S.-H. Recyclable, and Removable UV-Curable Coatings Derived from Tung Oil and Malic Acid. *Green Chem.* **2021**, *23* (16), 5875−5886.
(59) Tang, J.; Zhang, J.; Lu, J.; Huang, J.; Zhang, F.; Hu, Y.; Liu, C.; An, R.; Miao, H.; Chen, Y.; Huang, T.; Zhou, Y. Preparation and Properties of Plant-Oil-Based Epoxy Acrylate-like Resins for UV-Curable Coatings. *Polymers* **2020**, *12* (9), 2165.
(60) dos Santos, G. I.; Gaglieri, C.; Alarcon, R. T.; de Moura, A.; dos Santos, F. B.; Bannach, G. Glycerol and Maleic Anhydride-Based Acrylic Polyester: A Solution for Greener Photocurable Resins for 3D Printing of Renewable Materials. *ACS Sustainable Chem. Eng.* **2025**, *13* (25), 9771−9782.
(61) Wang, Y.; Xian, M.; Feng, X.; Liu, M.; Zhao, G. Biosynthesis of Ethylene Glycol from D-Xylose in Recombinant *Escherichia Coli*. *Bioengineered* **2018**, *9* (1), 233−241.
(62) Le Nôtre, J.; Witte-van Dijk, S. C. M.; van Haveren, J.; Scott, E. L.; Sanders, J. P. M. Synthesis of Bio-Based Methacrylic Acid by Decarboxylation of Itaconic Acid and Citric Acid Catalyzed by Solid Transition-Metal Catalysts. *ChemSuschem* **2014**, *7* (9), 2712−2720.
(63) Magri, R.; Gaglieri, C.; Alarcon, R. T.; Bannach, G. Epoxidation Reaction in Promising Brazilian Biomass: Decreased Time and Catalyst Loading to Produce Renewable Monomers. *J. Polym. Res.* **2021**, *28* (9), 343.
(64) Tu, J.; Makarian, K.; Alvarez, N. J.; Palmese, G. R. Formulation of a Model Resin System for Benchmarking Processing-Property Relationships in High-Performance Photo 3D Printing Applications. *Materials* **2020**, *13* (18), 4109.
(65) Bagheri, A.; Jin, J. Photopolymerization in 3D Printing. *ACS Appl. Polym. Mater.* **2019**, *1* (4), 593−611.
(66) Ou, X.; Huang, J.; Huang, D.; Li, X.; Chen, G.; Yang, Y.; Bi, R.; Sheng, Y.; Guo, S.Z. 4D-Printed Snake-like Biomimetic Soft Robots. *Bio-Des. Manuf.* **2025**, *8*, 55−67.
(67) Fu, P.; Li, H.; Gong, J.; Fan, Z.; Smith, A. T.; Shen, K.; Khalfalla, T. O.; Huang, H.; Qian, X.; McCutcheon, J. R.; Sun, L. 4D Printing of Polymers: Techniques, Materials, and Prospects. *Prog. Polym. Sci.* **2022**, *126*, 101506.
(68) Jeong, H. Y.; An, S. C.; Lim, Y.; Jeong, M. J.; Kim, N.; Jun, Y. C. 3D and 4D Printing of Multistable Structures. *Appl. Sci.* **2020**, *10* (20), 7254.
(69) Andreu, A.; Su, P.-C.; Kim, J.-H.; Ng, S. C.; Kim, S.; Kim, I.; Lee, J.; Noh, J.; Subramanian, A. S.; Yoon, Y.-J. 4D Printing Materials for Vat Photopolymerization. *Addit. Manuf.* **2021**, *44*, 102024.
(70) Pezzana, L.; Emanuele, A.; Sesana, R.; Delprete, C.; Malmström, E.; Johansson, M.; Sangermano, M. Cationic UV-Curing of Isosorbide-Based Epoxy Coating Reinforced with Macadamia Nut Shell Powder. *Prog. Org. Coat.* **2023**, *185*, 107949.
(71) Liguori, A.; Oliva, E.; Sangermano, M.; Hakkarainen, M. Digital Light Processing 3D Printing of Isosorbide- and Vanillin-Based Ester and Ester-Imine Thermosets: Structure-Property Recyclability Relationships. *ACS Sustainable Chem. Eng.* **2023**, *11* (39), 14601−14613.
(72) Frascella, F.; González, G.; Bosch, P.; Angelini, A.; Chiappone, A.; Sangermano, M.; Pirri, C. F.; Roppolo, I. Three-Dimensional Printed Photoluminescent Polymeric Waveguides. *ACS Appl. Mater. Interfaces* **2018**, *10* (45), 39319−39326.
(73) Zhao, T.; Yu, R.; Li, X.; Zhang, Y.; Yang, X.; Zhao, X.; Huang, W. A Comparative Study on 3D Printed Silicone-Epoxy/Acrylate Hybrid Polymers via Pure Photopolymerization and Dual-Curing Mechanisms. *J. Mater. Sci.* **2019**, *54* (6), 5101−5111.
(74) Gao, W.; Guo, Y.; Cui, J.; Liang, C.; Lu, Z.; Feng, S.; Sun, Y.; Xia, Q.; Zhang, B. Dual-Curing Polymer Systems for Photo-Curing 3D Printing. *Addit. Manuf.* **2024**, *85*, 104142.
(75) Kim, H. C.; Kwon, Y. R.; Kim, J. S.; So, J. H.; Kim, D. H. Dual-Cure Adhesives Using a Newly Synthesized Itaconic Acid-Based Epoxy Acrylate Oligomer. *Polymers* **2023**, *15* (15), 3304.
(76) Fernández-Francos, X.; Konuray, O.; Ramis, X.; Serra, À.; De la Flor, S. Enhancement of 3D-Printable Materials by Dual-Curing Procedures. *Materials* **2020**, *14* (1), 107.
(77) Ye, J.; Lin, G.; Lin, Z.; Deng, H.; Huang, J.; Xiang, H.; Rong, M. Z.; Zhang, M. Q. UV-Curable Polyurethane Elastomer with UV-Irradiation/Thermo Dual-Activated Self-Healability. *Macromol. Mater. Eng.* **2022**, *307* (6), 2100874.
(78) Lu, C.; Wang, C.; Yu, J.; Wang, J.; Chu, F. Two-Step 3D-Printing Approach toward Sustainable, Repairable, Fluorescent Shape-Memory Thermosets Derived from Cellulose and Rosin. *ChemSuschem* **2020**, *13* (5), 893−902.
(79) Ding, A.; Zhang, P.; Zhou, B.; Liu, G.; Xu, P.; Luo, Y.; Zhuang, Y.; Zhang, P.; Chen, A.; Liu, Y.; Luo, Z. Structural Design and Performance Study of a Biobased UV/Moisture Dual-Curing Coating for UV Inadequate Curing Conditions. *Mater. Today Commun.* **2025**, *44*, 111863.
(80) Yan, R.; Liu, Y.; Liu, B.; Zhang, Y.; Zhao, Q.; Sun, Z.; Hu, W.; Zhang, N. Improved Performance of Dual-Cured Organosolv Lignin-Based Epoxy Acrylate Coatings. *Compos. Commun.* **2018**, *10*, 52−56.
(81) Luo, Y.; Liu, G.; Xu, P.; Ding, A.; Zhang, P.; Zhang, P.; Mao, S.; Qiu, Z.; Xie, Z.; Mei, L. Structural Design and Preparation of LED/Moisture Dual-Cured Polyurethane Acrylate Coatings with Comprehensive Properties. *Prog. Org. Coat.* **2025**, *200*, 109080.
(82) Tu, R.; Sodano, H. A. Additive Manufacturing of High-Performance Vinyl Ester Resin via Direct Ink Writing with UV-Thermal Dual Curing. *Addit. Manuf.* **2021**, *46*, 102180.
(83) Luo, Y.; Liu, G.; Zhang, P.; Zhou, B.; Zhang, P.; Xu, P.; Qiu, Z.; Xie, Z.; Mei, L. Modified Castor Oil-Based UV/Thermal Dual-Curing Polyurethane Acrylate Coatings with Outstanding Comprehensive Properties. *Mater. Today Commun.* **2024**, *41*, 110978.
(84) Moradi, S.; Fernández-Francos, X.; Konuray, O.; Ramis, X. Recyclable Dual-Curing Thiol-Isocyanate-Epoxy Vitrimers with Sequential Relaxation Profiles. *Eur. Polym. J.* **2023**, *196*, 112290.
(85) Gaglieri, C.; Alarcon, R. T.; de Moura, A.; Bannach, G. Vegetable Oils as Monomeric and Polymeric Materials: A Graphical Review. *Curr. Res. Green Sustainable Chem.* **2022**, *5*, 100343.
(86) Sangermano, M.; Bergoglio, M.; Schögl, S. Biobased Vitrimeric Epoxy Networks. *Macromol. Mater. Eng.* **2024**, *309*, 2300371.
(87) Ferretti, F.; Damonte, G.; Cantamessa, F.; Arrigo, R.; Athanassiou, A.; Zych, A.; Fina, A.; Monticelli, O. On a Biobased Epoxy Vitrimer from a Cardanol Derivative Prepared by a Simple Thiol-Epoxy "Click" Reaction. *ACS Omega* **2024**, *9* (1), 1242−1250.
(88) Prudente, T. E. B.; Mauro, D.; Puig, J.; Altuna, F. I.; Da Ros, T.; Hoppe, C. E. Synthesis and Processing of Near Infrared—Activated Vitrimer Nanocomposite Films Modified with β-Hydroxyester-Functionalized Multi-Walled Carbon Nanotubes. *C* **2023**, *9* (4), 119.
(89) Rossegger, E.; Höller, R.; Reisinger, D.; Strasser, J.; Fleisch, M.; Griesser, T.; Schlögl, S. Digital Light Processing 3D Printing with Thiol-Acrylate Vitrimers. *Polym. Chem.* **2021**, *12* (5), 638−644.
(90) Du, L.; Wang, T.; Luo, S.; Liu, Z.; Wang, B.; Ma, Y.; Ren, S.; Jia, L.; Li, S. Lignin-Based Vitrimer Containing Dynamic Borate Ester

Bonds with Intrinsic Photoconversion and Excellent Photothermal Remoldability. *Int. J. Biol. Macromol.* **2024**, *278*, 134754.
(91) Ioannidis, R. O.; Bikiaris, N. D.; Vouvoudi, E.; Zamboulis, A.; Nikolaidis, N.; Bikiaris, D. N. Chemical Recycling of PLA and Its Copolyesters with Poly(Ethylene Azelate) via Microwave-Assisted Alkaline Hydrolysis and Enzymatic Hydrolysis. *Polymers* **2025**, *17* (10), 1374.
(92) Zheng, W. Z.; Li, X.; Xu, P. Y.; Zhang, Z. Y.; Wang, P. L.; Lu, B.; Huang, D.; Zhen, Z. C.; Ji, J. H.; Wang, G. X. Sustainable Recycling of the Biodegradable Polyester Poly(Butylene Succinate) via Selective Catalytic Hydrolysis and Repolymerization. *Resour., Conserv. Recycl.* **2024**, *209*, 107771.
(93) Bher, A.; Cho, Y.; Auras, R. Boosting Degradation of Biodegradable Polymers. *Macromol. Rapid Commun.* **2023**, *44* (5), 2200769.
(94) Alarcon, R. T.; Gaglieri, C.; Lamb, K. J.; North, M.; Bannach, G. Spectroscopic Characterization and Thermal Behavior of Baru Nut and Macaw Palm Vegetable Oils and Their Epoxidized Derivatives. *Ind. Crops Prod.* **2020**, *154*, 112585.
(95) Lanero, F.; Bresolin, B. M.; Scettri, A.; Nogarole, M.; Schievano, E.; Mammi, S.; Saielli, G.; Famengo, A.; Semenzato, A.; Tafuro, G.; Sgarbossa, P.; Bertani, R. Activation of Vegetable Oils by Reaction with Maleic Anhydride as a Renewable Source in Chemical Processes: New Experimental and Computational NMR Evidence. *Molecules* **2022**, *27* (23), 8142.
(96) dos Santos, G. I.; Gaglieri, C.; Alarcon, R. T.; Magri, R.; Hartlieb, M.; Bannach, G. Passion Fruit Seed Oil: A Sustainable Feedstock for Additive Manufacturing of Renewable Polymers. *J. Polym. Environ.* **2024**, *32*, 4748−4762.
(97) Kousaalya, A. B.; Ayalew, B.; Pilla, S. Photopolymerization of Acrylated Epoxidized Soybean Oil: A Photocalorimetry-Based Kinetic Study. *ACS Omega* **2019**, *4* (26), 21799−21808.
(98) Prat, D.; Wells, A.; Hayler, J.; Sneddon, H.; McElroy, C. R.; Abou-Shehada, S.; Dunn, P. J. CHEM21 Selection Guide of Classical- and Less Classical-Solvents. *Green Chem.* **2016**, *18* (1), 288−296.
(99) Colucci, G.; Stefano, F. D.; Sacchi, F.; Licciardello, M.; Tonda-Turo, C.; Lavagna, L.; Messori, M. Bio-Based Polymer Composites Obtained by Vat Photopolymerization of Photocurable Resins Modified with Biochar as Sustainable Filler. *Compos., Part A* **2025**, *198*, 109102.
(100) Liu, X.; Yang, X.; Wang, S.; Wang, S.; Wang, Z.; Liu, S.; Xu, X.; Liu, H.; Song, Z. Fully Bio-Based Polyhydroxyurethanes with a Dynamic Network from a Terpene Derivative and Cyclic Carbonate Functional Soybean Oil. *ACS Sustainable Chem. Eng.* **2021**, *9* (11), 4175−4184.
(101) Lin, T. W.; Mei, B.; Dutta, S.; Schweizer, K. S.; Sing, C. E. Molecular Dynamics Simulation and Theoretical Analysis of Structural Relaxation, Bond Exchange Dynamics, and Glass Transition in Vitrimers. *Macromolecules* **2025**, *58* (3), 1481−1497.
(102) Sun, Y.; Wang, X.; Zhao, Y.; Chen, X.; Shi, Q.; Jia, K. Temperature-Dependent Fracture Toughness of Epoxy Vitrimers. *Macromolecules* **2025**, *58* (2), 942−952.
(103) Lorenz, N.; Dyer, W. E.; Kumru, B. Exploring the Cure State Dependence of Relaxation and the Vitrimer Transition Phenomena of a Disulfide-Based Epoxy Vitrimer. *J. Polym. Sci.*. **2025**.
(104) Klein, F. C.; Sobania, N.; Abetz, V. Bio-Based Vinylogous Urethane Vitrimers from Waste-Wood Lignosulfonate and Enzymatic Lignin: Explorations in Stress Relaxation Behavior and Mechanical Strength. *J. Mater. Chem. A* **2025**, *13*, 29120−29137.
(105) Pezzana, L.; Melilli, G.; Delliere, P.; Moraru, D.; Guigo, N.; Sbirrazzuoli, N.; Sangermano, M. Thiol-Ene Biobased Networks: Furan Allyl Derivatives for Green Coating Applications. *Prog. Org. Coat.* **2022**, *173*, 107203.
(106) Pezzana, L.; Fadlallah, S.; Giri, G.; Archimbaud, C.; Roppolo, I.; Allais, F.; Sangermano, M. DLP 3D Printing of Levoglucosenone-Based Monomers: Exploiting Thiol-Ene Chemistry for Bio-Based Polymeric Resins. *ChemSuschem* **2024**, *17* (22), No. e202301828.
(107) Rosa, R. P.; Rosace, G.; Arrigo, R.; Malucelli, G. Preparation and Characterization of a Fully Biobased Resin System for 3d-Printing, Suitable for Replacing Fossil-Based Acrylates. *J. Polym. Res.* **2023**, *30* (4), 139.
(108) Gastaldi, M.; Cardano, F.; Zanetti, M.; Viscardi, G.; Barolo, C.; Bordiga, S.; Magdassi, S.; Fin, A.; Roppolo, I. Functional Dyes in Polymeric 3D Printing: Applications and Perspectives. *ACS Materials Lett.* **2021**, *3* (1), 1−17.
(109) Stevens, L. M.; Recker, E. A.; Zhou, K. A.; Garcia, V. G.; Mason, K. S.; Tagnon, C.; Abdelaziz, N.; Page, Z. A. Counting All Photons: Efficient Optimization of Visible Light 3D Printing. *Adv. Mater. Technol.* **2023**, *8* (23), 2300052.
(110) Ballester-Bayarri, L.; Pascal, A.; Ayestaran, J.; Gonzalez, A.; Ballard, N.; Aguirresarobe, R. 3D Printing of Vinylogous Urethane-Based Methacrylic Covalent Adaptable Networks by Vat Photopolymerization. *ACS Appl. Polym. Mater.* **2024**, *6* (5), 2594−2603.
(111) Guit, J.; Tavares, M. B. L.; Hul, J.; Ye, C.; Loos, K.; Jager, J.; Folkersma, R.; Voet, V. S. D. Photopolymer Resins with Biobased Methacrylates Based on Soybean Oil for Stereolithography. *ACS Appl. Polym. Mater.* **2020**, *2* (2), 949−957.
(112) Fouassier, J. P.; Morlet-Savary, F.; Lalevée, J.; Allonas, X.; Ley, C. Dyes as Photoinitiators or Photosensitizers of Polymerization Reactions. *Materials* **2010**, *3* (12), 5130−5142.
(113) Pierau, L.; Elian, C.; Akimoto, J.; Ito, Y.; Caillol, S.; Versace, D. L. Bio-Sourced Monomers and Cationic Photopolymerization−The Green Combination towards Eco-Friendly and Non-Toxic Materials. *Prog. Polym. Sci.* **2022**, *127*, 101517.
(114) Li, P.; Ma, S.; Dai, J.; Liu, X.; Jiang, Y.; Wang, S.; Wei, J.; Chen, J.; Zhu, J. Itaconic Acid as a Green Alternative to Acrylic Acid for Producing a Soybean Oil-Based Thermoset: Synthesis and Properties. *ACS Sustainable Chem. Eng.* **2017**, *5* (1), 1228−1236.
(115) Pawelzik, P.; Carus, M.; Hotchkiss, J.; Narayan, R.; Selke, S.; Wellisch, M.; Weiss, M.; Wicke, B.; Patel, M. K. Critical Aspects in the Life Cycle Assessment (LCA) of Bio-Based Materials - Reviewing Methodologies and Deriving Recommendations. *Resour., Conserv. Recycl.* **2013**, *73*, 211−228.
(116) Terry, J. S.; Taylor, A. C. The Properties and Suitability of Commercial Bio-Based Epoxies for Use in Fiber-Reinforced Composites. *J. Appl. Polym. Sci.* **2021**, *138* (20), 50417.
(117) Dai, J.; Ma, S.; Wu, Y.; Zhu, J.; Liu, X. High Bio-Based Content Waterborne UV-Curable Coatings with Excellent Adhesion and Flexibility. *Prog. Org. Coat.* **2015**, *87*, 197−203.
(118) He, W.; Huang, H.; Xie, L.; Wang, C.; Yu, J.; Lu, S.; Fan, H. The Influence of Self-Crosslinked Epoxidized Castor Oil on the Properties of Poly (Lactic Acid) via Dynamic Vulcanization: Toughening Effect, Thermal Properties and Structures. *Colloids Surf., A* **2021**, *630*, 127517.
(119) Liu, T.; Hao, C.; Wang, L.; Li, Y.; Liu, W.; Xin, J.; Zhang, J. Eugenol-Derived Biobased Epoxy: Shape Memory, Repairing, and Recyclability. *Macromolecules* **2017**, *50* (21), 8588−8597.
(120) Sölle, B.; Shaukat, U.; Rossegger, E.; Schlögl, S. Synthesis and Characterization of Bio-Based Transesterification Catalysts for Green 3D-Printable Dynamic Photopolymers. *Polym. Chem.* **2023**, *14* (44), 4994−5003.
(121) Liu, J.; Zhang, C.; Li, Z.; Zhang, L.; Xu, J.; Wang, H.; Xu, S.; Guo, T.; Yang, K.; Guo, K. Dibutyl Phosphate Catalyzed Commercial Relevant Ring-Opening Polymerizations to Bio-Based Polyesters. *Eur. Polym. J.* **2019**, *113*, 197−207.
(122) Delahaye, M.; Winne, J. M.; Du Prez, F. E. Internal Catalysis in Covalent Adaptable Networks: Phthalate Monoester Transesterification As a Versatile Dynamic Cross-Linking Chemistry. *J. Am. Chem. Soc.* **2019**, *141* (38), 15277−15287.
(123) Vazquez-Martel, C.; Becker, L.; Liebig, W. V.; Elsner, P.; Blasco, E. Vegetable Oils as Sustainable Inks for Additive Manufacturing: A Comparative Study. *ACS Sustainable Chem. Eng.* **2021**, *9* (49), 16840−16848.

https://doi.org/10.1021/acssuschemeng.5c07154
ACS Sustainable Chem. Eng. 2025, 13, 16136−16153